Copyright © by

OLAV LOUIS HANSEN

1972

THERMAL RADIATION FROM THE GALILEAN SATELLITES MEASURED AT 10 AND 20 MICRONS

Thesis by

Olav Louis Hansen

In Partial Fulfillment of the Requirements

for the Degree of

Doctor of Philosophy

California Institute of Technology

Pasadena, California

1972

(Submitted May 22, 1972)

ACKNOWLEDGMENTS

I thank Dr. James Westphal, my thesis advisor, for suggesting the study of infrared eclipse phenomena of the Galilean satellites. At every stage of this project, from conception to completion, Dr. Westphal has given generously of his time and experience.

I also thank Messrs. Solomon Giles, Victor Nenow, and Devere Smith for their aid in the design and construction of equipment, and the staffs at Mt. Wilson and Palomar observatories for their help during the observing phase.

The outcome of this work has been influenced by stimulating discussions with Dr. Eric Becklin about data analysis, Dr. Bruce Murray about satellite surfaces, Dr. Dennis Matson about calibration procedures, my colleague Mr. William Ward about thermal models, and Dr. James Westphal about interpretating the results.

I thank Dr. Gerry Neugebauer for contributing greatly to my education as an "infrared" observer.

For reading manuscrips of the thesis, and offering many constructive suggestions, I am indepted to Dr. Eric Becklin, Dr. Andrew Ingersoll, Dr. Dennis Matson, Dr. Bruce Murray, Dr. Gerry Neugebauer, and Dr. James Westphal.

A very personal thanks goes to Dr. Bruce Murray and my wife, Elizabeth, who jointly persuaded me to continue my studies after the first year at C.I.T. had undermined my selfconfidence.

The writer was supported by an Earle C. Anthony Fellowship and a C.I.T. Research Foundation Fellowship. The research expenses were covered under NASA Grant 05002003.

ABSTRACT

The four Galilean Satellites have been observed in two broad bandpasses, centered near 10μ and 20μ respectively, during Jupiter's 1971-apparition.

Two types of measurements were obtained. The first consisted of monitoring the infrared flux as a function of each satellite's orbital position, the other of flux measurements during satellite eclipses. The latter type was obtained only in the 10μ bandpass, and only for Io (J1), Europa (J2), and Ganymede (J3), because Callisto (J4) was not eclipsed in 1971.

The flux measurements obtained as a function of orbital position were averaged for each satellite and bandpass, and from the mean values the following quantities were derived: (1) the maximum (~subsolar) surface temperature, T_{max}, (2) the ratio between the effective 20μ emissivity, ϵ_{20}, and the effective 10μ emissivity, ϵ_{10}, (3) the bolometric Bond albedo, A_{bol}, and (4) the effective phase integral, q. The results, listed in Table (i), indicate very low "$\epsilon_{20}/\epsilon_{10}$" ratios and high q-values.

TABLE (i)

THERMAL PARAMETERS OF THE GALILEAN SATELLITES: 1

Satellite	T_{max}	$\epsilon_{20}/\epsilon_{10}$	A_{bol}	q
J1	146 ± 5°K	0.58 ± 0.12	0.47 ± 0.08	0.84 ± 0.13
J2	136 ± 5	0.62 ± 0.12	0.60 ± 0.06	0.87 ± 0.09
J3	150 ± 5	0.67 ± 0.13	0.41 ± 0.09	1.02 ± 0.22
J4	161 ± 5	0.72 ± 0.14	0.20 ± 0.11	1.2 ± 0.6*

*From other considerations, the lower limit appears more plausible.

The 10μ flux measurements obtained during eclipses of J1, J2, and J3 have been compared to thermal models, and the following conclusions were drawn. (1) No homogeneous model [single parameter, $\gamma = (k\rho c)^{-\frac{1}{2}}$] can

account for the observed temperature variations during eclipses. (2) A two-layer model with a thin, thermally insulating layer covering a highly conductive subsurface is adequate to explain all the observations. (3) The atmospheric surface pressure on J1, J2, and J3 is less than 1 mbar. (4) The results, listed in Table (ii), show that the surface covering of J1 is distinctly different from that of J2 or J3.

TABLE (ii)

THERMAL PARAMETERS OF THE GALILEAN SATELLITES: 2 TWO-LAYER MODEL

Satellite	Top Layer			Subsurface
	$\gamma \left(\frac{^\circ K\ cm^2\ sec^{\frac{1}{2}}}{cal}\right)$	$k \left(\frac{\mu Watt}{cm\ ^\circ K}\right)$	τ(cm)	k
J1	1100 ± 100	32 ± 7	0.37 ± 0.06	Like that of solid rock or dense ice
J2	3000 ± 1000	4 ± 3	0.2 ± 0.1	
J3	3400 ± 700	4 ± 1	0.22 ± 0.06	

$\gamma = (k\rho c)^{-\frac{1}{2}}$, k = thermal conductivity and ρ, c, and τ are respectively the density, specific heat and thickness of the top layer.

TABLE OF CONTENTS

TABLE OF CONTENTS

TABLE OF CONTENTS

FIGURES

TABLE OF CONTENTS

TABLES

TABLE OF CONTENTS

TABLES (Continued)

I. INTRODUCTION

a) Motivation

In the last decade, the four Galilean satellites of Jupiter have undergone fairly intensive investigation. The current interest has probably been triggered by the prospect of sending probes to Jupiter, but that is not the sole justification which comes to mind.' Firstly, each of the Galilean satellites is as large as the Moon and should, from a geological viewpoint, be just as interesting. Yet, due to their remoteness, the state of knowledge about the Galilean satellites is miniscule compared with that of the Moon. Secondly, just as the Moon is becoming a key to understanding the evolution of the terrestrial planets, so might the Galilean satellites become keys to understanding the Jovian planets. That is to say, the Galilean satellites are not just duplicates of the Moon placed in orbit about Jupiter. Their evolution has been governed by an entirely different environment than that of terrestrial planets. It is not too much to hope for, that their past history has left an imprint on their surfaces. By compiling observational data coupled with carefully made inferences, one can therefore hope that a decipherable pattern will eventually emerge.

This thesis deals with the thermal emission from the satellites. To place the findings in perspective, a brief review of previous investigations is necessary.

b) Summary of Previous Work

(i) Investigations of Reflected Light

Most observers have preferred to study the properties of light reflected by the satellites in order to obtain knowledge of the satellite surfaces and test

for the presence of atmospheres. The first quantitative photometry was carried out by Stebbins (1927) and Stebbins and Jacobsen (1928). Employing a broad bandpass, which spanned the visible spectrum, these authors measured light curves of the satellites with periods corresponding to their orbital periods about Jupiter. They were thus the first to demonstrate that all four satellites are in synchronous rotation. At the same time they also measured the solar phase function out to the limit of ± 12 degrees imposed by the relative positions of the Sun, Jupiter and the Earth. The phase functions showed the characteristic backscatter peak, near zero phase angle, which now is called the "opposition effect" after Gehrels (1956) and Gehrels, Coffeen and Owings (1964) discovered that some asteroids and the Moon showed this effect. Harris (1961) brought UBV photometry to bear on the satellites and discovered that J1 (Io), J2 (Europa) and J3 (Ganymede) are highly reflecting in the V*-bandpass (especially J1) and strongly absorbing in the U-bandpass. J4 (Callisto) is more Moon-like in its reflectivity. Narrow band photometry has been carried out by McNamara (1964), Moroz (1966), Johnson (1971), and Johnson and McCord (1971). Although no definite identification of surface materials has been possible, due to a lack of known, characteristic absorbsion features, important constraints have been obtained: The reflectivity curves of J2 and J3 decrease beyond 1 μ. This behavior is consistent with spectra of frosts but not of common silicates. Also the total reflectivity of J1, J2, and J3 is frost-like, i.e. much higher than that of common silicates. Yet, the absorbsion in the ultraviolet, exibited by all the satellites, is not characteristic of frosts. The possibility that the surfaces consist

*The effective wavelengths of the U, B, and V filters used by Harris were 0.353, 0.448, and 0.554 μ.

of a material which does not occur naturally on Earth should not be dismissed. The polarization measurements by Veverka (1971) should also be mentioned here. Only J4 shows a pronounced negative branch, similar to that of the Moon. Veverka interprets the absence of negative branches for J1, J2, and J3 to mean that the surfaces of these three satellites consist of bright, low-opacity materials.

So far, spectroscopic searches for atmospheres have had negative results. Searches were carried out by Kuiper (1952), Owen (1965), Kalinyak (1966), and Binder and Cruikshank (1966). Of these only Kalinyak has reported finding any non-solar absorbsion lines. Binder and Cruikshank addressed themselves to the validity of Kalinyak's findings and concluded that the lines he had found corresponded to weak solar lines. Spectroscopy is of course limited to volatiles which have detectable absorbsion features. Another method which has been employed in search of atmospheres is eclipse-photometry. The ploy is to look for temporary frost deposits just after eclipse. While the method is limited to those volatiles which would saturate in the atmosphere due to the temperature decrease during an eclipse, it is sensitive to very small amounts ($\approx 10^{-3}$ mbar surface pressure) of such volatiles. The results of this type of search have been somewhat confusing. In 1964 Binder and Cruikshank noticed an "overshoot" in the brightness of J1 just after it reappeared from eclipse. If the signal intensity is measured as a function of time, one would expect it to increase monotonically from zero, as the satellite reappeared from eclipse, and approach a constant value assymptotically. Instead, they measured an increase from zero which overshot their final value by about 10%. The overshoot "decayed" in about 15 minutes. They interpreted the "excess brightening" as being caused by a temporary frost, deposited during the eclipse,

which evaporated on a timescale of ca. 15 minutes. In 1965 they observed a similar but smaller (~3%) excess from J2. Johnson (1971) verified the excess brightening of J1 in two narrow bandpasses near 4350 Å and 5600 Å, finding it to be greater at the shorter wavelength. On the other hand, Fallon and Murphy (1970) as well as Franz and Millis (1970) have searched repeatedly for excess brightening of J1 with negative results. O'Leary and Veverka (1970) have measured an excess brightening of J1, but qualify their findings by casting doubt on the sensitivity of the standard photometric technique (single beam) employed. The main difficulty lies in subtracting the scattered light from Jupiter. It appears that Franz and Millis, using a rapid scan technique, have devised the most sensitive method for subtracting the "sky signal" from the observed signal. If so, one must conclude either that the earlier determinations were in error or that the phenomenon is time dependent.

(ii) Investigations of Thermal Radiation

Only recently has it become technologically feasible to measure the thermal radiation from the Galilean satellites. Brightness temperatures, or related quantities, have been reported by Murray, Wildey and Westphal (1964), Low (1965), Gillett, Merrill and Stein (1970), Matson (1972), and Morrison, Cruikshank and Murphy (1972). Typical values run from 130°K to 150°K in the sequence: J2, J1, J3, J4. Matson was the first to measure a variation with orbital phase angle for J3 and J4. His work has been extended in this thesis to all four satellites in broad bandpasses at 10 and 20 μ.

Infrared photometry during satellite eclipses offers still another way to search for atmospheres. The method is based on the fact that the thermal

conductivity of the surface material increases with ambient gas pressure. Because of its direct relevance to this thesis, the method will be discussed in detail later. At the time of writing, only eclipse results from J3 have been reported. The first measurement was obtained by Murray, Westphal and Wildey (1965) at 10μ. This was repeated at 20μ by Morrison et al. (1971). Both measurements set an upper limit on the surface pressure of J3 at 1 mbar. Eclipses of J1 and J2 have now also been measured; at 20μ by Morrison et al. (private communication), and at 10μ by this author. Part IV of this thesis deals with the results.

(iii) Investigation of Bulk Properties

The satellite masses have been estimated by de Sitter (1931) on the basis of mutual orbit perturbations. In his paper, de Sitter reviews three of his own calculations as well as individual calculations by Laplace, Damoisean, Adams, and Sampson. The reader should be warned that there are large, unexplained (Marsden, private communication) discrepancies in the mass determinations of J1 and J4.

The satellite radii have been obtained by several methods, direct and indirect. These methods and the results have been reviewed by Dollfus (1970). The radius of J1 has since been measured with high precision during the β Sco C occultation (Taylor et al. 1972), and found to be 1830 ± 3 km - which is about 130 km larger than the mean value based on the review by Dollfus. The measurements are discussed in section "III a".

J1 apparently modulates the decametric emission from Jupiter's magnetic field (Bigg, 1964). An explanation of this effect has been suggested by Goldreich and Lynden-Bell (1969), requiring an electrical conductivity $\sigma \gg 10^{-8}$ ohm^{-1}cm^{-1} of J1. In contrast, the conductivity of the outer

"skin" of the Moon is less than 10^{-9} ohm^{-1}cm^{-1}(Dyal and Parkin, 1971). However, below the insulating layer, the Moon's conductivity is greater than 10^{-4} ohm^{-1}cm^{-1}, and it is entirely possible that J1 could have the required conductivity.

Lewis (1971) has discussed the satellite interiors on the basis of their densities, which vary from 2.8 to 1.4 for J1 → J4, and the chemical composition in the solar nebula. According to Lewis "the Galilean satellites of Jupiter...very likely have extensively melted interiors, and most probably contain a core of hydrous silicates, an extensive mantle of ammonia-rich liquid water, and a relatively thin crust of ices". On that note we leave the summary of previous work.

c) Aims and Approach

The goal of this investigation has been to provide data on such surface properties as can be derived from infrared photometry. These properties are the surface temperature, the infrared emissivity, the bolometric Bond albedo, the effective phase integral, the thermal inertia, and the presence or absence of atmospheres on J1, J2, and J3.

The approach has been the following: (i) The thermal flux signal from each satellite has been measured in two broad bandpasses, centered at 10 and 20μ, as a function of orbital phase angle. (ii) The signals have been calibrated against known standards to yield absolute flux densities at the effective wavelengths of the bandpasses. (iii) The mean flux density in each bandpass has been converted to a brightness temperature, and the effective emissivity ratio between the two bandpasses has been calculated. (iv) The mean flux densities and the emissivity ratio have been used to estimate the maximum surface temperature, the bolometric Bond albedo, and the effective phase

integral. (v) Eclipses of J1, J2, and J3 have been observed through the 10μ bandpass to yield cooling and heating curves. (vi) Thermal models have been investigated, and agreement between the observed and the predicted eclipse curves has been demonstrated for one type of model. That model consists of a thin ($\approx$mm) highly insulating layer on top of a semi-infinite, highly conducting subsurface. And (vii) from that model the thermal conductivity and thickness of the top layer has been determined and compared to laboratory data.

II. OBSERVATIONS

a) Equipment

The equipment used in this work consisted of the following parts: a double beam photometer, a liquid helium dewar containing a cooled filter wheel, limiting aperture, field lens, galium doped germanium bolometer and load resistor; a preamplifier, a phase-lock amplifier, a stripchart recorder in parallel with a voltage to frequency converter (VFC), and a frequency counter with printer.

The photometer elements are sketched in Figure 1. Note that the filter wheel is cooled to liquid nitrogen temperature, while the limiting aperture, field lens, detector, and load resistor are cooled below the λ-point of helium (2°K) by pumping. The bolometer and preamplifier were purchased from the Arizona Research Laboratory. The photometer and helium dewar were constructed at C.I.T. Three broad band filters, centered approximately at 5, 10, and 20μ, were available. However, only the 10 and 20μ filters were employed on the satellites. The two bandpasses are shown in Appendix (d).

The electronic equipment is shown in Figure 2, a flow diagram, indicating the function of each piece.

b) Data Reduction

(i) Method of Measurement

Except for eclipse data, to be described separately, all the satellite and calibration data were obtained at the Cassegrain (f/16) focus of the 60 inch Hale Observatory telescope on Mt. Wilson.

The photometer was operated so as to produce a difference-signal from two neighboring spots of the sky at a frequency of 15 Hz. The aperture was

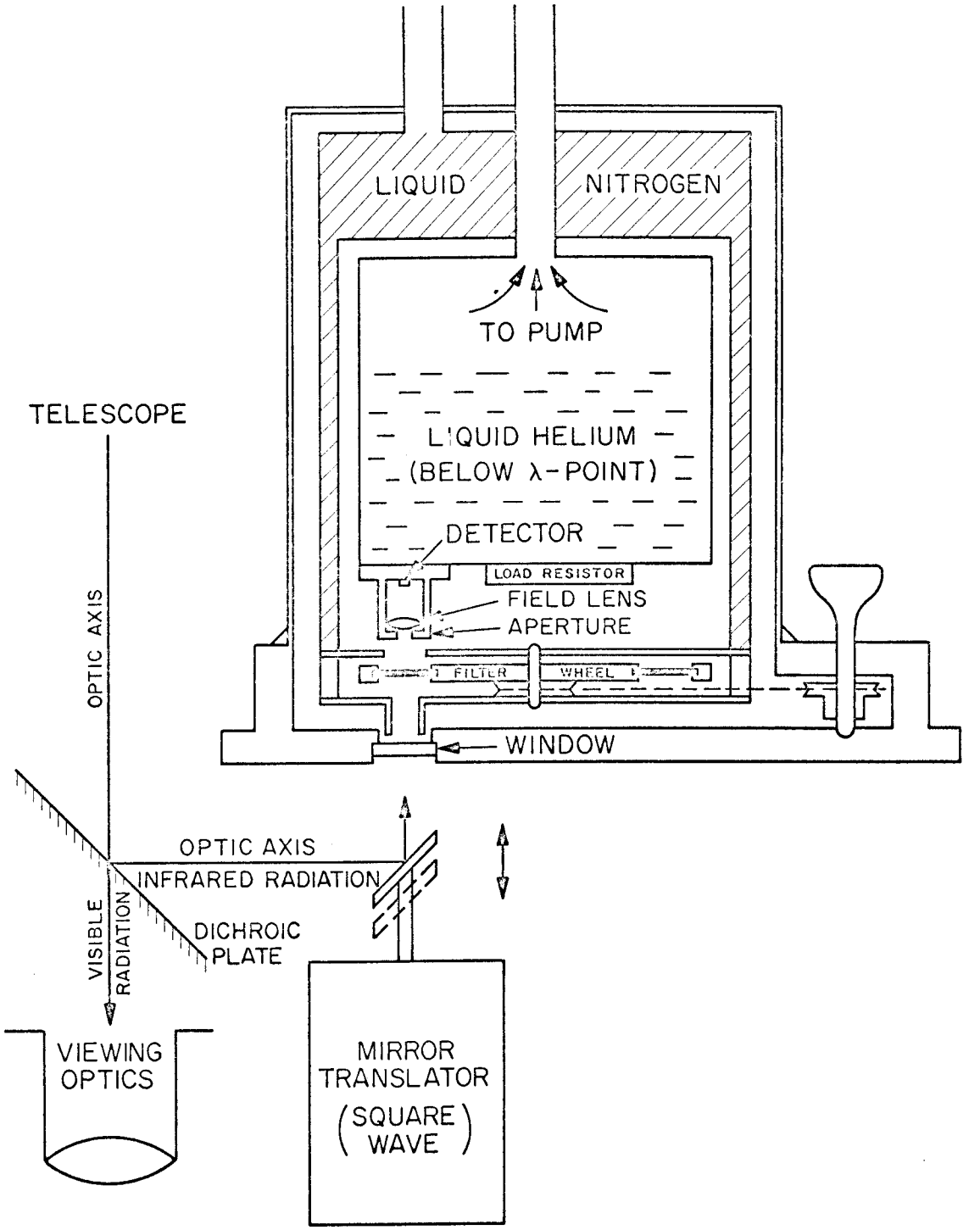

Fig. 1 - Working elements of photometer. Not shown to scale.

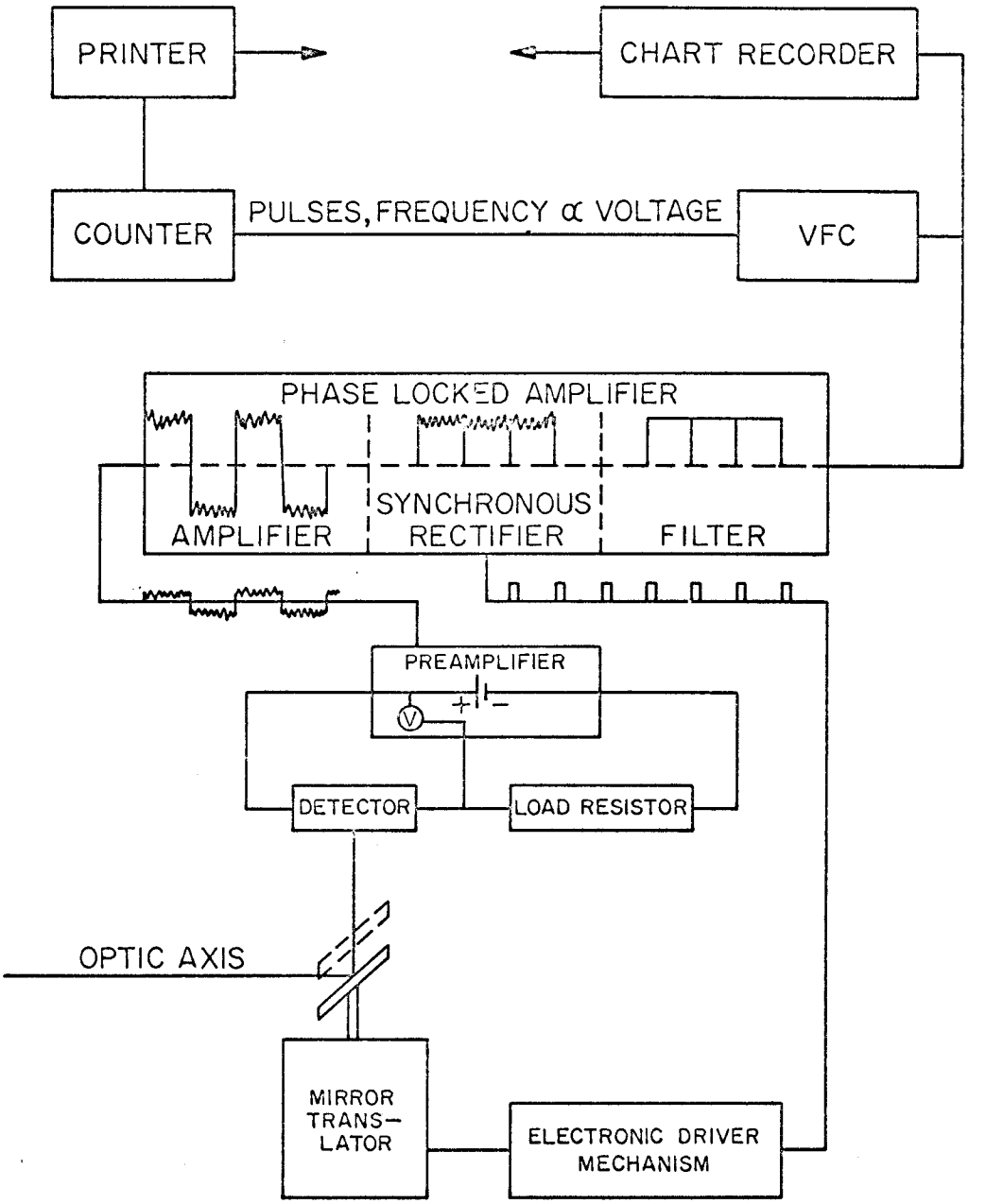

Fig. 2. - Electronic equipment. Waveforms are indicated on the leads.

10 arcseconds in diameter and the beam separation was about 12 arcseconds center to center. The following steps define a "measurement": a count, c_k, was obtained by placing the source in one beam and integrating the pulses from the VFC for 10 seconds. Successive counts were produced by alternating the source between the two beams, and the counts were used to form a set of differences, $\{-(c_1 - c_2),\ +\ (c_2 - c_3),\ -\ (c_3 - c_4), + \ldots\}$. Finally a measurement, S, and its standard deviation, ϵ, were obtained by averaging the differences and evaluating their variation. The number of differences making up a measurement varied between 3 and 19, depending on the signal strength, with 5 being typical.

(ii) Standard Star Observations

On each observing night usually two, and often four, calibration stars were measured. Table 1 lists the stars measured for calibration and the number of times an independent flux ratio in a given bandpass between any two stars were obtained. For each flux ratio between star "i" and star "j", measured on the same night, a relative magnitude, m_{ij}, and a weight, w_{ij}, were assigned according to

$$m_{ij} = -2.5 \log_{10} S_i/S_j - \alpha(A_i - A_j) \qquad (1)$$

$$w_{ij} = (1 - \tfrac{1}{2}|A_i - A_j|)/(\epsilon_i^2 + \epsilon_j^2) \qquad (2)$$

where S_k is a measurement (previously defined) of the k'th star

A_k is the airmass at which the star was observed

ϵ_k is the standard deviation in the measurement

and α is the extinction coefficient for the relevant bandpass. If one or more stars were measured more than once during a night, then a weighted

mean, $\langle m \rangle_{ij}$, was obtained to replace m_{ij} for the night, in order that all the relative magnitudes used in the overall average should be independently determined.

Rather than apply different extinction coefficients for each night, average values were adopted. They were $\alpha = 0.28$, 0.10, 0.80 magnitudes per airmass for the 5, 10, and 20μ bandpasses. Only in the case of the 20μ bandpass, could serious error occur due to an error in α. However, all the 20μ satellite data were compared to αSco, which was near Jupiter in 1971, so that the airmass difference did not exceed 0.4 airmasses. Thus a 30% error in α would cause less than a 10% error in the satellite flux determination.

At the completion of the observing program for this study, an overall average was found. For each set of relative magnitudes a weighted mean, $\langle m_{ij} \rangle$, was calculated. The means of the relative magnitudes were then correlated to yield the magnitude of each star relative to αLyr. This correlation led to small internal inconsistencies which were minimized by slight adjustments of the $\langle m_{ij} \rangle$ values. The residuals, defined by

$$r_{ij} = \langle m_{ij} \rangle \text{ adjusted} - \langle m_{ij} \rangle \text{ original} \qquad (3)$$

are shown in Figure 3. They are generally of the order of 0.03 and never greater than 0.07 magnitudes. Because αLyr was below the detection limit of the 20μ bandpass, a value of -4.69 magnitudes was adopted for αSco. This choice was based on an independent 20μ flux calibration which will be discussed later. The results of the calibration measurements are given in Table 2 together with the largest standard deviation in $\langle m_{ij} \rangle$ affecting a particular value. It is difficult to compare these results to those of other observers because the exact form of each bandpass varies between systems. The

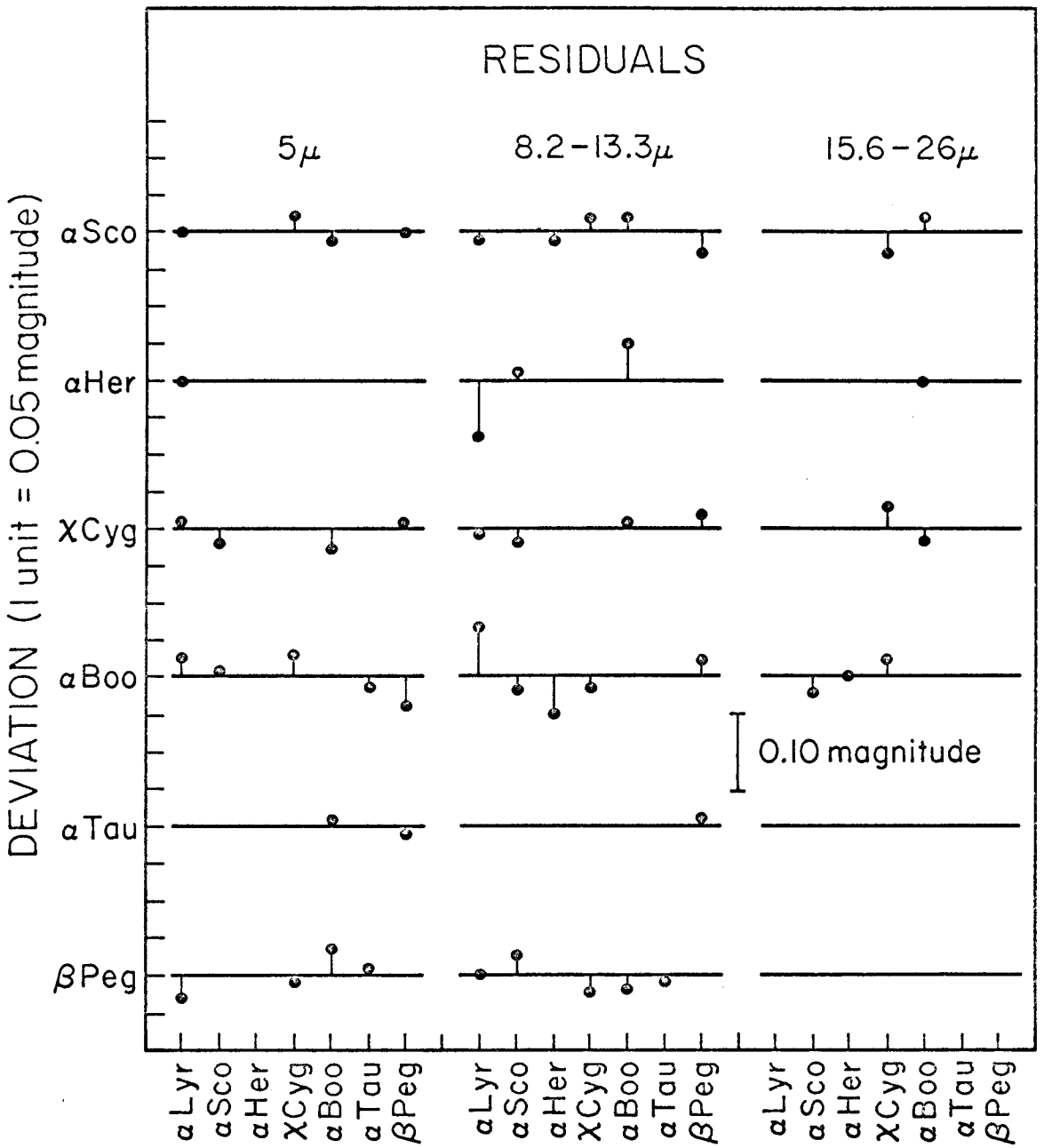

Fig. 3. - Residuals from the magnitude correlation procedure.

current practice in infrared astronomy is for each observer to measure a set of calibration stars relative to α Lyr, or some other standard, with the identical system that he intends to use for further quantitative work. For a recent review of measurements by other observers in the 8 - 14μ atmospheric "window", the reader is referred to Matson (1972).

TABLE 1

NUMBER OF INDEPENDENT RATIOS OBTAINED BETWEEN CALIBRATION STARS

STAR RATIO	Bandpass		
	5μ	10μ	20μ
α Lyr - α Sco	3	2	0
- α Her	3	3	0
- α Boo	1	3	0
- β Peg	3	3	0
- χ Cyg	2	3	0
α Sco - α Her	0	1	0
- α Boo	1	6	4
- β Peg	2	2	0
- χ Cyg	1	1	2
α Boo - α Her	0	4	1
- β Peg	2	3	0
- χ Cyg	1	2	2
- α Tau	1	2	0
β Peg - χ Cyg	2	3	0
- α Tau	1	1	0

TABLE 2

MAGNITUDES OF CALIBRATION STARS

OBJECT	Bandpass 5μ	10μ	20μ
α Lyr	≡0.00	≡0.00	
α Sco	-3.85 ± 0.05	-4.41 ± 0.10	-4.69(Adopted)
α Her	-3.40 ± 0.05	-3.93 ± 0.12	-3.50 ± ?
α Boo	-2.84 ± 0.05	-2.95 ± 0.10	-3.10 ± 0.09
β Peg	-2.17 ± 0.07	-2.37 ± 0.08	-2.79 ± ?
χ Cyg (May 22-24,'71)	-2.57 ± 0.08	-3.55 ± 0.09	-4.24 ± 0.06
α Tau	-2.90 ± ?	-2.95 ± 0.09	

(iii) Satellite Data Reduction

We shall now regard the magnitudes of the calibration stars as known. To obtain the magnitude of one of the satellites at a given time, we go back to the original data for the night and assign a system sensitivity, β_i, to each calibration measurement according to

$$\beta_i = m_i + (2.5 \log_{10} S_i + \alpha A_i) \tag{4}$$

where m_i is the adopted magnitude of the i'th calibration star. The k'th satellite magnitude, adjusted to an Earth-Jupiter distance of 4.2 a.u. is given by

$$m_k = -2.5 \log_{10} S_k - \alpha A_k + \langle \beta \rangle - 5 \log_{10} (D/4.2 \text{ a.u.}) \tag{5}$$

where $\langle \beta \rangle$ is the mean of the $\{\beta_i\}$ set for that night, and D is the distance between the Earth and Jupiter.

The m_k's obtained during all the observing nights are shown in Figures 4 and 5 as a function of orbital phase angle* The smooth curves shown in the

*The orbital phase angle is the longitude of the satellite seen from Jupiter's North pole, with zero taken at superior conjunction of the satellite as seen from the Earth.

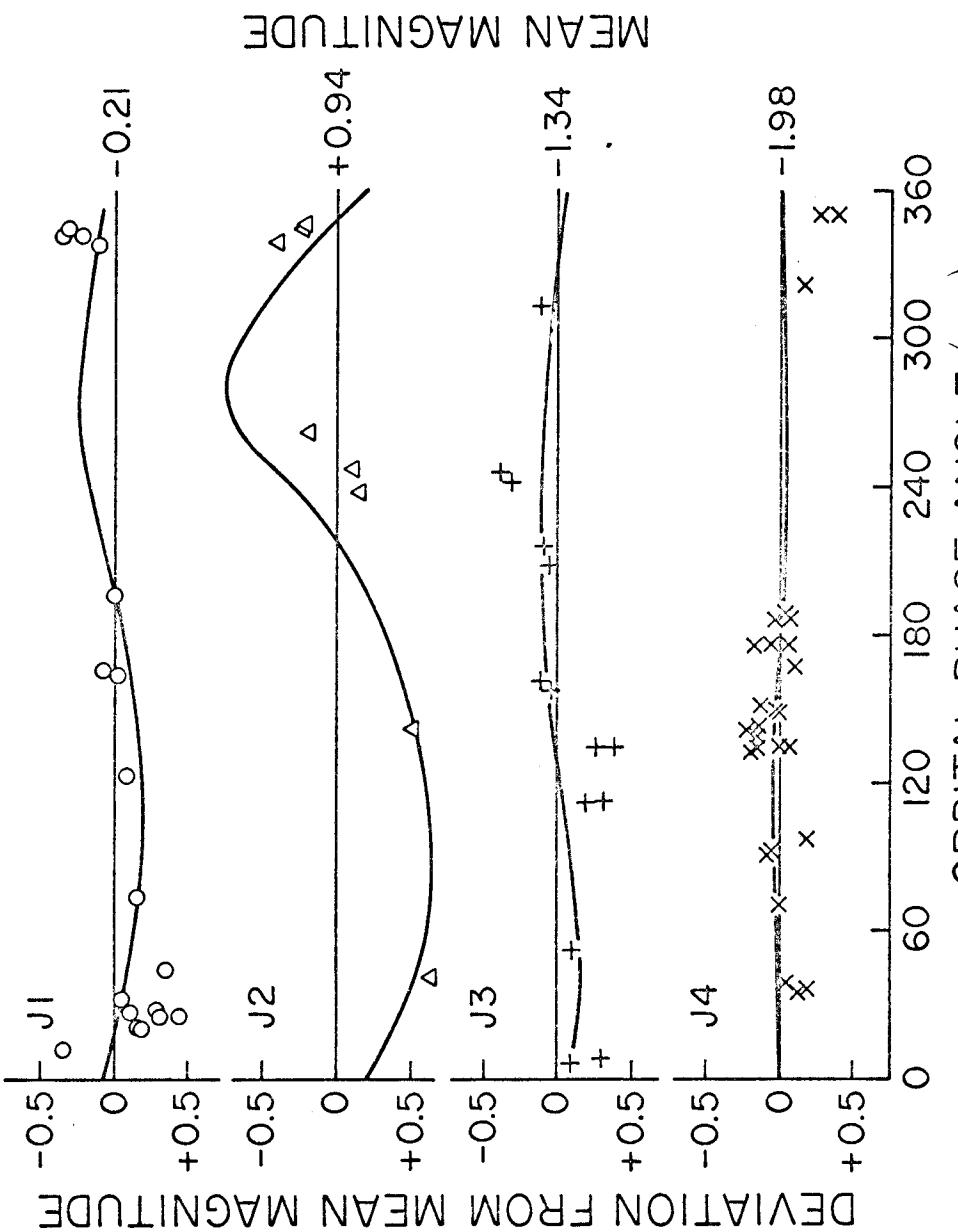

Fig. 4. - Satellite magnitudes in the 10μ bandpass. Variation with orbital phase angle. Smooth curves are predicted infrared (10μ) orbital phase angle curves based on visible photometry data from Stebbins and Jacobsen (1928).

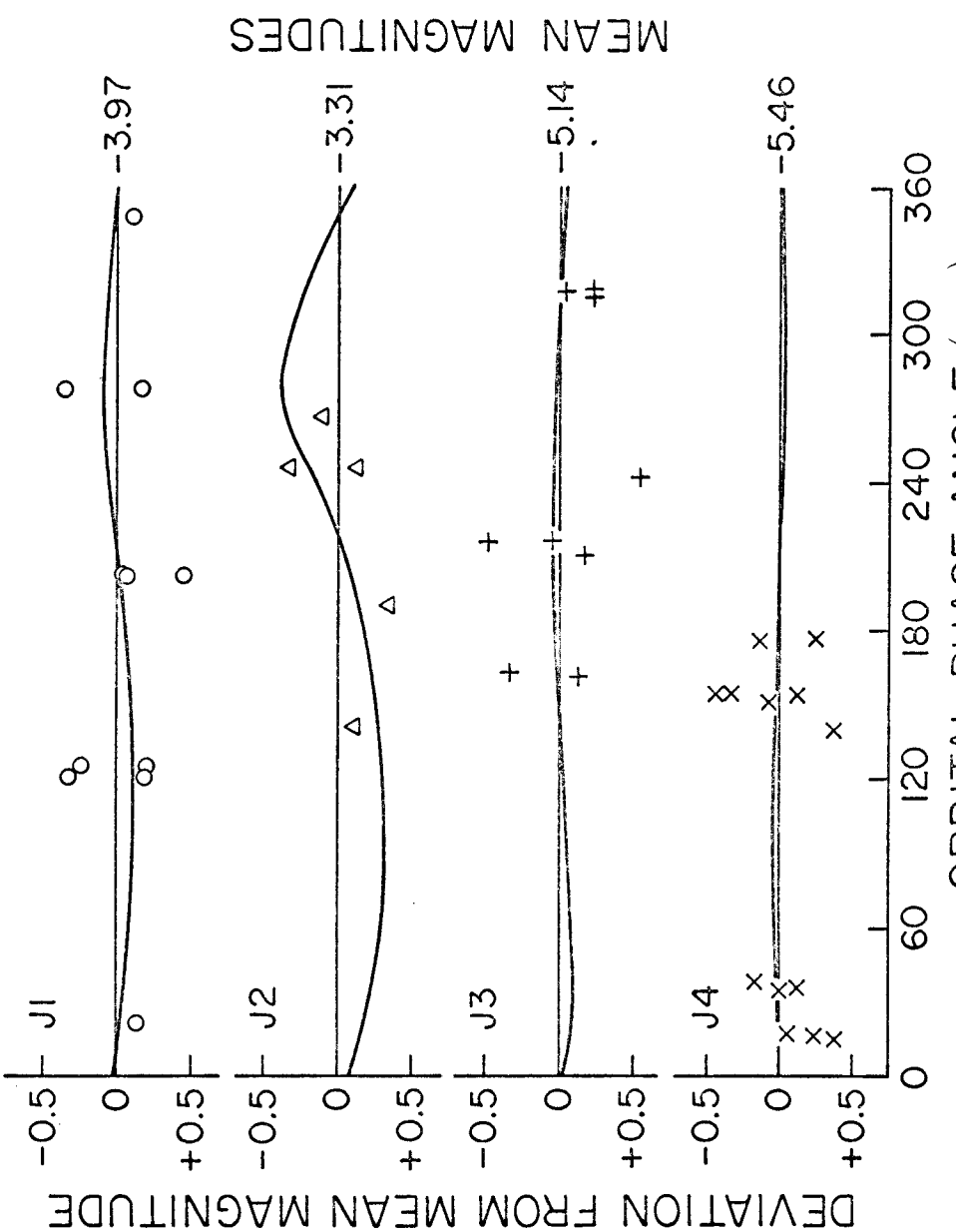

Fig. 5. - Satellite magnitudes in the 20μ bandpass. Variation with orbital phase angle. Smooth curves are predicted infrared (20μ) orbital phase angle curves based on visible photometry data from Stebbins and Jacobsen (1928).

figures are derived from a simple model applied to the visible photometry data of Stebbins and Jacobsen (1928). Although more recent data exist, see Harris (1961) and Johnson (1971), the older data have been preferred here because the broad bandpass used by Stebbins and Jacobsen corresponds roughly to an integration over the solar energy spectrum, and that is exactly what one wants for this application. In brief, the model consisted of assuming that the brightness temperature would vary with the observed albedo changes according to

$$T^4(\psi) \propto [1 - A(\psi)], \tag{6}$$

where ψ is the orbital phase angle. From that assumption it is easily shown that the infrared magnitude should vary with orbital phase angle as

$$m(\psi) = m(o) + \frac{z\gamma}{\lambda T(o)} \left\{ \left[\frac{1 - A(o)}{1 - A(\psi)} \right]^{\frac{1}{4}} - 1 \right\} \tag{7a}$$

where $$A(\psi) = A(o) \exp \left\{ [n(o) - n(\psi)]/z \right\} \tag{7b}$$

and $\gamma = hc/k = 14413 \mu^{\circ}K$

λ = Wavelength denoting the bandpass

$z = 2.5/2.3026$

n = visual magnitude

ψ = o represents the orbital phase angle at which $n(\psi)$ equals the mean visual magnitude.

While this model may be oversimplified, it is clear that the scatter in the infrared data is too large to justify a more sophisticated model. Matson (1972) was the first to attempt to measure the infrared orbital phase curves of the two brightest (IR) Galilean satellites, J3 and J4. Working with narrow bandpasses in the 8 - 14μ atmosphere window, he observed variations as

large as ±0.6 magnitudes in the 8.5μ bandpass for J4. Such a large variation is difficult to reconcile with the model above and the 10μ data obtained in this work.

The main purpose of measuring the satellite flux as a function of orbital phase angle is not, however, to pin down the exact form of the variation, but to insure that a fair sample is used in obtaining mean magnitudes for further analysis. Anticipating the need to know mean fluxes rather than mean magnitudes, the following quantity has been calculated for each satellite and bandpass:

$$m \equiv \log \langle \log^{-1} (m_k) \rangle \quad , \tag{8}$$

and used as the "mean magnitude" in plotting $m_k(\psi)$. "$\langle\ \rangle$" implies an average over the set $\left\{\log^{-1} (m_k)\right\}$. Values for m are listed in Table 3. The uncertainity in these values is difficult to assess because the noise is superimposed on a real variation. Judging from the uncertainty in the calibration measurements, which is about 0.1 magnitude, one might expect a similar uncertainty here.

TABLE 3

MEAN MAGNITUDES OF THE GALILEAN SATELLITES

Bandpass	J1	J2	J3	J4
10μ	-0.21	+0.94	-1.34	-1.98
20μ	-3.97	-3.31	-5.14	-5.46

1) All magnitudes adjusted to an Earth-Jupiter distance of 4.2 a.u.
2) The uncertainty in both bandpasses is about 0.10 to 0.15 magnitude.

c) Effective Wavelengths

Although wide band photometry is a useful tool for studying radiation too weak for narrow band photometry, results are often difficult to interpret.

It is easy to conceive of sources with spectral features within the pass band of the instrument which could cause an erroneous interpretation of the measurements. Within the scope of this work, it has been necessary to assume that the emission spectra of α Lyr near 10μ, and of Mars and the Galilean satellites near 10μ and near 20μ are featureless within the respective pass bands.

The concept of the effective wavelength of a bandpass is a time saving devise corresponding to integrating the flux spectrum of a source over the instrumental bandpass. Let $B(\lambda, T)$ be the flux spectrum of a source at temperature T, and let S be the instrumental response to the source in a particular bandpass. Then S is given by

$$S = \alpha \int_0^\infty B(\lambda,T)\ \varphi(\lambda)\ d\lambda \tag{9}$$

where α is a proportionality constant, and $\varphi(\lambda)$ is the normalized system response i.e. the transmission of the atmosphere, window, and filter together with the reflectivity of the telescope mirrors, and the efficiency of the detector. The effective wavelength, λ_{eff}, of a bandpass, $a \leq \lambda \leq b$, is defined by that solution to the equation

$$B(\lambda_{eff}, T) = \int_a^b B(\lambda, T)\ \varphi(\lambda)\, d\lambda \Big/ \int_a^b \varphi(\lambda)\, d\lambda \tag{10}$$

for which $a \leq \lambda_{eff} \leq b$.

In order to calculate λ_{eff} one needs to know $\varphi(\lambda)$ and $B(\lambda,T)$. Since we wish to deal with sources for which $B(\lambda,T)$ is unknown we shall assume that the sources behave as black bodies within the bandpass of interest. Then $B(\lambda, T)$ is the Planck function, and λ_{eff} (T) may be calculated as a function of source temperature. In the calculations $\varphi(\lambda)$ has been taken to be

$$\varphi(\lambda) = a(\lambda)\ w(\lambda)\ f(\lambda)\ b(\lambda) \tag{11}$$

where $a(\lambda)$ = atmospheric transmission from Farmer and Key (1965)

$w(\lambda)$ = window transmission (2mm KBr)

$f(\lambda)$ = filter transmission (from manufacturer). See Appendix (d).

$b(\lambda)$ = bolometer response assumed uniform.

The function $\lambda_{eff}(T)$ is difficult to use because it is ill behaved for flux spectra which peak close to the bandpass. To avoid the problem one may define a correction factor, C(T), which will permit the use of a constant wavelength $\lambda_o = \lambda_{eff}(T\rightarrow\infty)$ in place of $\lambda_{eff}(T)$. C(T) is defined by

$$B(\lambda_o, T) = C(T)\ B(\lambda_{eff}\ (T),\ T). \tag{12}$$

$\lambda_{eff}(T)$ and C(T) are shown in Figure 6 for the 10μ bandpass used in this work. Note that $C_o = C(T\rightarrow\infty) = 1$. It is important to realize that C(T) represents a small correction to the measured flux density of a source at a temperature different than the standard source temperature. Our assumption, that the sources behave as black bodies, in this calculation, therefore introduces only a negligible error in the results. this may be clarified by an example.

Suppose we wish to calculate the flux density at λ_o of a disk* at temperature T, area πR^2, and a distance D away. Let $B(\lambda_o, T_o)$ be the known "zero magnitude flux density" from αLyr, and let "m" be the measured magnitude of the disk relative to αLyr in the bandpass corresponding to λ_o. The desired flux density at λ_o, $B(\lambda_o, T)/C(T)$, is then given by

$$\frac{\pi R^2}{D^2}\left[\frac{B(\lambda_o, T)}{C(T)}\right] = \left[\frac{B(\lambda_o, T_o)}{1}\right] \times 10.^{-m/2.5} \tag{13}$$

*The angular size of the disk is assumed to be small with respect to the beam pattern.

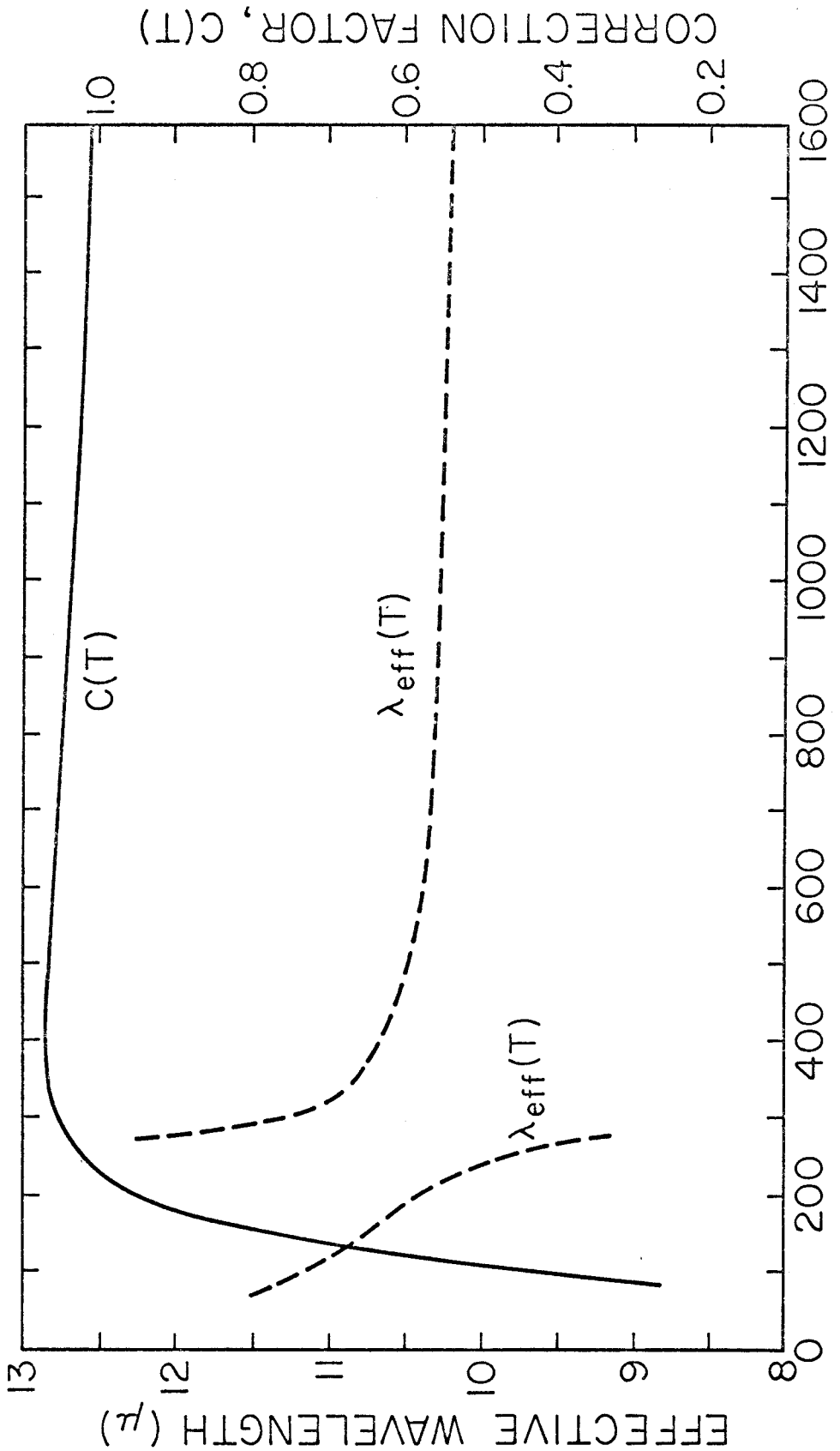

Fig. 6. - Effective wavelength and correction factor as functions of source temperature for the 10μ bandpass.

Note that the black body - assumption applies neither to the zero magnitude flux density, nor to $B(\lambda_0, T)$. Only C(T) contains that assumption as a second order effect.

Another problem with wide band photometry is the airmass dependence of the system response. Since the bandpass spans numerous atmospheric absorbsion features, the effective wavelength for a given source temperature should change with airmass. This problem has been investigated under a simplifying assumption. Let $y(z,\lambda)$ be the transmission of the atmosphere at airmass z and wavelength λ. The assumption is that $y(z,\lambda)$ behaves with airmass according to

$$y(z,\lambda) = e^{-k(\lambda)z} = y(z=1,\lambda)^z \quad . \tag{14}$$

Because broadening of absorbsion features has been ignored, this is perhaps not a very good approximation to the actual behavior of $y(z,\lambda)$. It is nevertheless encouraging to note that, within the stated assumption, the investigation showed the effect to be negligible for airmasses less than 2.5 and source temperatures greater than 80°K. Calculations of $\lambda_{eff}(T)$ and C(T) were carried out for the 20μ bandpass at 1.0 and 2.5 airmasses. In the latter case, the magnitude error, Δm, incurred by neglecting the "airmass effect" was calculated. The results are listed in Table 4 together with $\lambda_{eff}(T)$ and C(T) from the 10μ bandpass at 1 airmass.

TABLE 4

EFFECTIVE WAVELENGTHS AND CORRECTION FACTORS

Source Temperature (°K)	Bandpass 8.2 - 13.3μ, 1 Airmass λ_{eff}	C(T)	Bandpass 15.6 - 26.0μ, 1 Airmass λ_{eff}	C(T)	Bandpass 15.6 - 26.0μ, 2.5 Airmass λ_{eff}	C(T)	Δm
80	11.39	0.261	20.97	0.835	20.60	.867	0.040
90	11.28	0.353	20.68	0.908	20.39	.925	0.020
100	11.17	0.445	20.41	0.958	20.18	.965	0.009
110	11.08	0.529	20.10	0.992	19.96	.992	0.000
120	10.99	0.607	19.70	1.016	19.66	1.011	-0.006
140	10.84	0.732	18.09	1.045	18.36	1.033	-0.012
160	10.69	0.831	21.83	1.057	21.35	1.042	-0.015
200	10.41	0.952	20.90	1.062	20.55	1.046	-0.016
250	9.84	1.025	20.58	1.058	20.30	1.044	-0.015
275	9.21 or 12.16	1.044	20.49	1.055	20.23	1.041	-0.014
300	8.29 11.38	1.057	20.43	1.052	20.18	1.038	-0.014
350	10.84	1.067	20.34	1.046	20.11	1.034	-0.013
500	10.49	1.067	20.20	1.031	20.01	1.024	-0.008
1000	10.28	1.037	20.08	1.014	19.93	1.013	-0.002
10000	10.16	1.000	20.00	1.000	19.86	1.000	-0.000

d) Flux Calibration

The visible flux from αLyr has been measured by Oke and Schild (1970) relative to a standard source to yield an absolute calibration at 0.5480μ. Subsequently, Schild, Peterson and Oke (1971) proposed a stellar atmosphere model for B and A stars that included an extrapolation out to 21μ for αLyr. Adopting that calibration, one finds the zero magnitude flux density for the effective wavelengths, evaluated for a 10,000° K black body source, to be the following:

TABLE 5

ZERO MAGNITUDE FLUX DENSITIES

λ_o	$B(\lambda_o, T_o)$
4.80μ	17.53×10^{-16} Watt/cm^{2}μ
10.16	1.096 "
20.00	0.0751 "

Because αLyr can be measured reliably at wavelengths shorter than 14μ, this calibration can be applied directly for the 5 and 10μ bandpasses by measuring an unknown source relative to αLyr. Other calibration stars are necessary only as intermediaries to distribute the calibration spatially over the entire sky. At longer wavelengths, however, one encounters difficulty in detecting αLyr, and a new, detectable standard must be found and calibrated. Neugebauer, Becklin, and Hansen (1972) have calibrated αSco relative to Mars and obtained a flux density from αSco of $(5.4 \pm 0.5) \times 10^{-16}$ Watt/cm^{2}μ at 20.00μ. If the flux density from αLyr at 20μ is as predicted by the αLyr model, then the flux density measurement from αSco implies a magnitude of αSco equal to -4.7 ± 0.1 relative to αLyr.

e) Satellite Flux Densities

The mean flux densities in the 10 and 20μ bandpasses may now be calculated for each satellite. The results are listed in Table 6. Beware of the C(T) - factor which has not been taken out of the measurements. Only after the temperature has been found can the factor be removed. In other words, a few iterations are necessary before the temperature can be determined, but convergence is rapid due to the weak temperature dependence of C(T).

TABLE 6

SATELLITE FLUX DENSITIES

Band-pass	$F_\lambda \times 10^{16}$ (Watt/cm^{2}μ) J1	J2	J3	J4
10μ	1.3 ± 0.1	0.46 ± 0.05	3.8 ± 0.4	6.8 ± 0.7
20μ	2.9 ± 0.3	1.6 ± 0.2	8.5 ± 0.9	11.5 ± 1.0

To make a clear distinction between the measured and the calculated flux densities, the symbol "F_λ" shall be used for the former, and the symbol "$B(\lambda_o, T)/C(T)$" for the latter.

III. INTERPRETATION

Under certain assumptions, which will be introduced in context, the results of the last chapter may be used to derive the following quantities: The 10 and 20μ brightness temperatures, the ratio between the 10 and 20μ emissivities, the maximum surface temperature, the bolometric Bond albedo, and the effective phase integral. Two important results are derived: (1) The 20μ emissivities are significantly less than the 10μ emissivities for all four satellites. (2) The effective phase integrals of J1, J2 and J3 are considerably higher than those of the Moon and Mercury.

a) Preliminaries

(i) Satellite Radii

Dollfus (1970) has reviewed a number of radius determinations published between 1827 and 1961, and obtained by a variety of techniques. A breakdown of the methods employed follows: Double image micrometry (7 observers), interferometry (3), filament micrometry (11), eclipse photometry (2), and discometry (1). The scatter of values within any one method is as high as 25%, and there appears to be systematic differences between methods as well. Since the review, the radius of J1 has been measured with high precision during the occultation of β Sco C. Several groups cooperated in a worldwide effort, and have published a preliminary note (Taylor et al. 1972) giving a value of 1830±3 km to the equatorial radius of J1. In order to use this determination as a normalization for the other three satellites, the previous measurements have been graphed in a "smoothed histogram" as follows: To each published radius value of J1 was assigned a Gaussian curve of equal height and standard deviation, with its center located at the reported radius on a radius-axis. Figure 7 shows the sum of these curves plotted as a

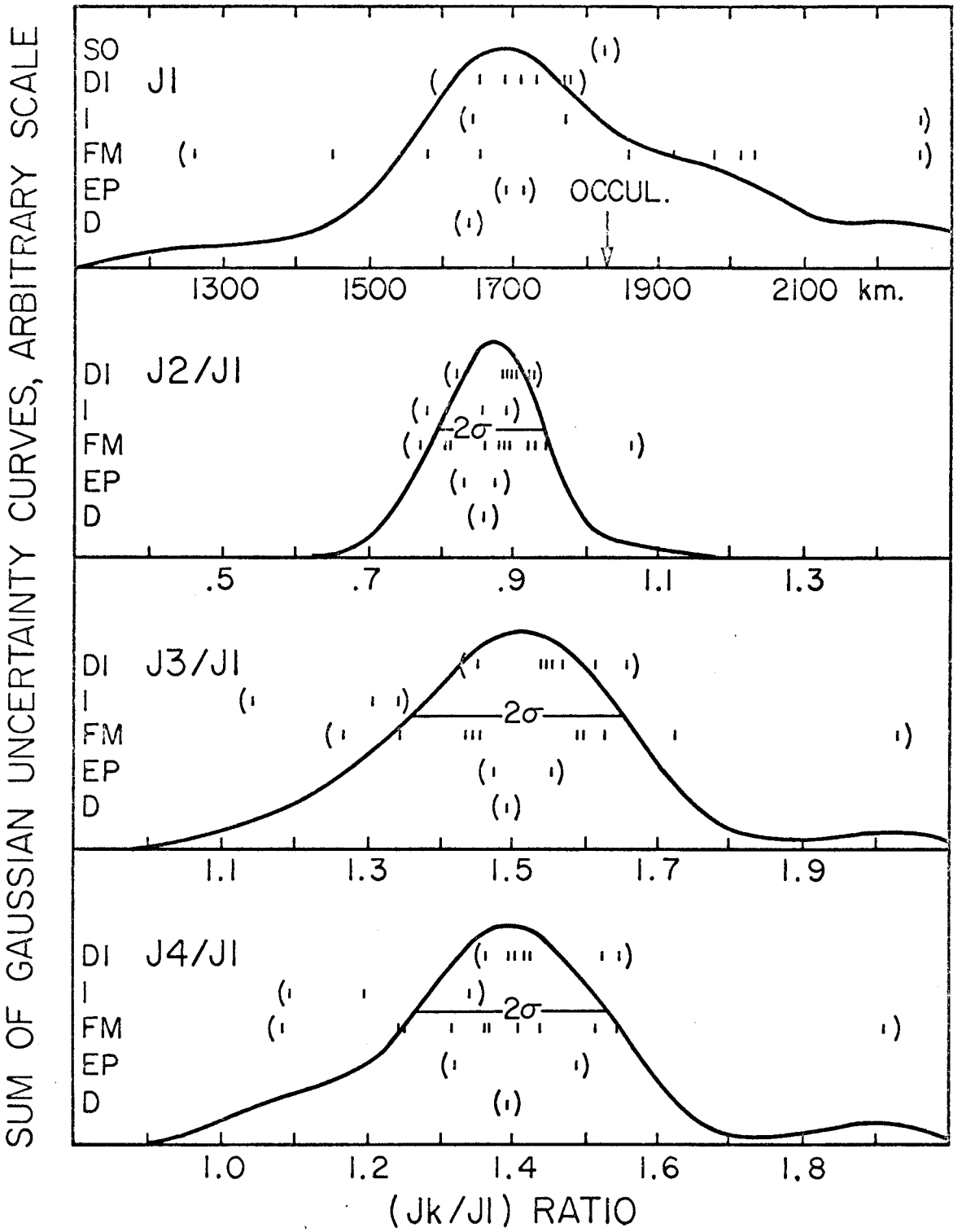

Fig. 7. - Distribution of Satellite Radii Measurements. Abbreviations for the various techniques are: SO (Stellar Occultation), DI (Double Image), I (Interferometry), FM (Filament Micrometer), EP (Eclipse Photometry), D (Discometer). Tickmarks indicate individually published measurements. Data from a review by Dollfus (1970).

function of radius. For J2, J3, and J4 the ratio "Jk/J1" was used instead of the radius itself in order to remove systematic differences in the various methods. Figure 7 also shows the original data points separated into groups according to method of observation. We have adopted the following ratios: J2/J1 = 0.88, J3/J1 = 1.51, J4/J1 = 1.39. If we also adopt the "occultation radius" for J1, we obtain R = 1830, 1610, 2760, 2550 km for J1→J4. The uncertainty in the latter 3 values is difficult to assess. If the histogram curves are thought of as quasi-Gaussian, then one standard deviation away from the peak corresponds to ≈10% of the radius. Since 24 independent measurements have been used, the standard deviation of the mean is ≈2%. If this criterion of uncertainty is used, one obtains R = 1830±3, 1610±30, 2760±60, and 2550±50 km. Two recent radius determinations for J2 and J3 have been omitted from the analysis because the approach required a ratio between the radius of the satellite and that of J1. Both determinations were obtained from eclipse photometry. They were: R(J2) = 1200±100 km (Greene, Shorthill, and Despain, 1971), and R(J3) = 2200±100 km (Price and Hall, 1971). Both of these are lower than the adopted values, but fall well within the scatter in the other individual measurements.

(ii) Geometric Albedos

The geometric albedos of the Galilean satellites have been measured between 0.3μ and 2.5μ by Johnson and McCord (1971) and Moroz (1966). The measurements have been extended to 5μ by Gillett, Merrill and Stein (1970). Data past 2.5μ are, however, not important for this discussion because the insolation becomes negligible beyond that wavelength. The geometric albedos are shown in Figure 8 together with the solar energy spectrum, $S(\lambda)$, taken from Arvesen, Griffin, and Pearson (1969). Straight line

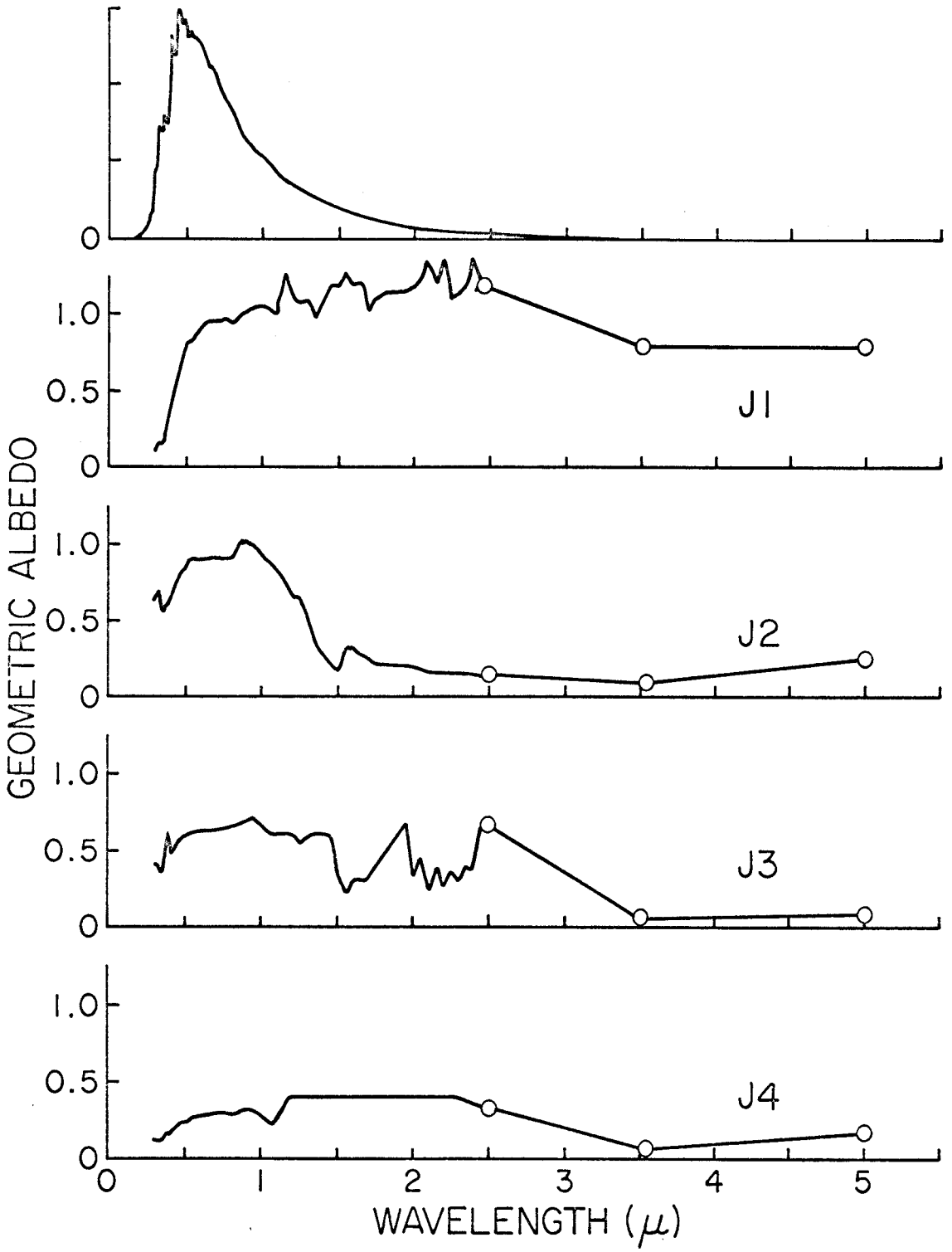

Fig. 8. - Solar energy spectrum, from Arvesen et al. (1969), and geometric albedos of the satellites, from Johnson and McCord (1971), Moroz (1966), and Gillett et al. (1970), as functions of wavelength.

segments are linear interpolations between two given values. It is useful to calculate an effective geometric albedo, p_{eff}, defined by

$$p_{eff} = \int_0^\infty p(\lambda)\ S(\lambda)\ d\lambda \Big/ \int_0^\infty S(\lambda)\ d\lambda \qquad (15)$$

where $p(\lambda)$ is the geometric albedo.

In making a determination of $p(\lambda)$, an observer measures $p(\lambda)R^2$ and deduces $p(\lambda)$ by adopting a value for R. This usage is unfortunate because each observer prefers his own "adopted" radius. The radii adopted to determine $p(\lambda)$ were lower than the ones used in this work, because the observers did not have the benefit of the "occultation radius" of J1. The reported geometric albedos have therefore been multiplied by a correction factor, k, given by

$$k = (R_1/R_2)^2 \qquad (16)$$

where R_1 is the radius used to derive $p(\lambda)$, and R_2 is the corresponding radius used in this work. The effective geometric albedos are listed in Table 7.

TABLE 7

EFFECTIVE GEOMETRIC ALBEDOS

	R_1 (km)	R_2 (km)	k	p_{eff}
J1	1686	1830	0.85	0.56
J2	1505	1610	0.87	0.69
J3	2340	2760	0.72	0.40
J4	2285	2550	0.80	0.17

(iii) The Bolometric Bond Albedos

The bolometric Bond albedo, A_{bol}, is defined as the ratio between the

total energy reflected by a planet and the total energy incident on a planet per unit time. It is obtained by weighting the wavelength dependent Bond albedo by the solar energy spectrum, i.e.

$$A_{bol} = \int_0^\infty A(\lambda)\ S(\lambda)\ d\lambda \Big/ \int_0^\infty S(\lambda)\ d\lambda \quad . \tag{17}$$

$A(\lambda)$ has been discussed by Harris (1961) in terms of the geometric albedo, $p(\lambda)$, and the phase integral, $q(\lambda)$. The discussion shall be repeated here for convenience.

Consider a rectangular coordinate system, centered in the planet, with z-axis toward the Sun and with the Earth in the x-z plane. Assume axial symmetry in the reflected radiation about the z-axis, and let $\Phi(\theta,\lambda)\, d\Omega\, d\lambda$ be the radiation in the wavelength interval $\lambda \to \lambda + d\lambda$ reflected by the planet into a solid angle $d\Omega$ in direction θ. Then $A(\lambda)$ is given by

$$A(\lambda) = \int_0^{2\pi} \int_0^{\pi} \Phi(\theta,\lambda) \sin\theta\ d\theta\ d\varphi\ d\lambda \Big/ \pi R^2\ S(\lambda)\ d\lambda \tag{18}$$

where the numerator is the energy in the wavelength interval $\lambda \to \lambda + d\lambda$ reflected in all directions, and the denominator is the incident energy in the same wavelength interval.

Let $$j(\theta,\lambda) = \Phi(\theta,\lambda) \Big/ \Phi(o,\lambda) \tag{19}$$

then $$A(\lambda) = \frac{2\Phi(o,\lambda)}{R^2 S(\lambda)} \int_0^{\pi} j(\theta,\lambda) \sin\theta\ d\theta \quad . \tag{20}$$

The geometric albedo, $p(\lambda)$, and the phase integral, $q(\lambda)$, are defined to be

$$p(\lambda) = \Phi(o,\lambda) / R^2 S(\lambda) \tag{21}$$

$$q(\lambda) = 2 \int_0^{\pi} j(\theta,\lambda) \sin\theta\ d\theta \tag{22}$$

$$\Rightarrow A(\lambda) = p(\lambda)\, q(\lambda). \tag{23}$$

Hence $$A_{bol} = \int_0^\infty q(\lambda)\, p(\lambda)\, S(\lambda)\, d\lambda \Big/ \int_0^\infty S(\lambda)\, d\lambda. \tag{24}$$

$p(\lambda)$ can be obtained for any planet either by measuring $\Phi(0,\lambda)$, or by extrapolating $\Phi(\theta,\lambda)$ to zero phase angle. To determine $q(\lambda)$, on the other hand, one must view the planet at all phase angles: $0 \leq \theta \leq 180^\circ$. This is possible only for inferior planets and the Moon. For Jupiter and its satellites, the largest phase angle attainable from Earth-based observations is ca. 12°. $j(\theta,\lambda)$ can therefore be obtained only for phase angles at which the multiplying factor, $\sin\theta$, is near zero, so even a crude estimate of $q(\lambda)$ is impossible.

Since the bolometric Bond albedo determines the energy balance of the planet, one can derive an indirect estimate for A_{bol}, and hence the phase integral, from a measurement of the surface temperature. For this purpose we shall define the "effective phase integral", q_{eff}, by

$$q_{eff} \int_0^\infty p(\lambda)\, S(\lambda)\, d\lambda \equiv \int_0^\infty q(\lambda)\, p(\lambda)\, S(\lambda)\, d\lambda \quad . \tag{25}$$

Then, from the previous definition of "effective geometric albedo" one obtains

$$A_{bol} = q_{eff}\, p_{eff} \quad . \tag{26}$$

b) Brightness Temperatures and Emissivity Ratio

The brightness temperature, T_b, in each bandpass, denoted by λ, is given by

$$F_\lambda = \frac{\pi R^2}{D^2} \quad \frac{B(\lambda_o, T_b)}{C(T_b)} \tag{27}$$

where F_λ is the measured flux density in the bandpass, and $B(\lambda_o, T_b)$ is the Planck function evaluated at λ_o = 10.16 or 20.00μ, at temperature $T_b(10\mu)$ or $T_b(20\mu)$. $C(T_b)$ is the correction factor, mentioned earlier, which adjusts $B(\lambda_o, T_b)$ to $B[\lambda_{eff}(T_b), T_b]$. R is the satellite radius and D = 4.2a.u. The results, listed in Table 8, show that the brightness temperature is lower at 20μ than at 10μ by about 10°K, for each satellite. This corresponds to a "deficiency" in the flux density at 20μ relative to that at 10μ of 30-40%. We can think of 4 explanations which might in part or wholly account for the "discrepancy".

(i) That the satellite measurements relative to the calibration sources are in error. This explanation seems unlikely, especially for J1, J3, and J4 in view of the many individual measurements obtained, under a variety of atmospheric conditions, most of which fall within 10% of the predicted infrared orbital phase angle curves.

(ii) That either the 10μ or the 20μ calibration is in error. The calibration referred to earlier assumed that the ratio $\epsilon_{20}/\epsilon_{10}$* was known for Mars. That assumption was based on the Mariner '69 experiment (Neugebauer et al. 1971) which yielded $\epsilon_{20}/\epsilon_{10} = 0.98 \pm 0.03$. Since the Mars calibration applied equally to the 10 and 20μ bandpasses, it is unlikely that there could be a 30-40% relative error between the 10 and 20μ calibrations.

(iii) That ϵ_{20} is lower than ϵ_{10} for each of the Galilean satellites. While this is an unexpected result, one can offer no logical

*Here and elsewhere, ϵ_λ shall stand for the effective emissivity obtained in the bandpass denoted by λ.

argument against it without knowing the physical and chemical form of the surface materials.

(iv) That the directivity of the emissivity is a function of wavelength, so as to make ϵ_{20} appear lower than ϵ_{10} as viewed from the Earth. This explanation cannot be distinguished from (iii) on the basis of observational evidence unless spacial resolution over the satellite disks is obtained.

To proceed, we shall assume that the third explanation holds. The emissivity ratio can then be calculated by assuming that the effective surface temperature is equal to the 10μ brightness temperature. Had we chosen the 20μ brightness temperature, we should have obtained an even lower emissivity ratio. Thus

$$\frac{\epsilon_{20}}{\epsilon_{10}} = \left(\frac{F_{20}}{F_{10}}\right)\left[\frac{B(10.16,\ T)}{B(20.00,\ T)}\right]\left[\frac{C_{20}(T)}{C_{10}(T)}\right] \tag{28}$$

If we assume a 10% uncertainty in both F_{10} and F_{20}, the maximum error possible in $\epsilon_{20}/\epsilon_{10}$ is 20%. The results are listed in Table 8.

TABLE 8

BRIGHTNESS TEMPERATURES AND EMISSIVITY RATIOS

Object	Bandpass 10μ T_b(°K)	10μ $C(T_b)$	Bandpass 20μ T_b(°K)	20μ $C(T_b)$	$\left(\frac{\epsilon_{20}}{\epsilon_{10}}\right)$
J1	137	0.715	124	1.02	0.58±0.12
J2	127	0.657	117	1.01	0.62±0.12
J3	140	0.732	130	1.03	0.67±0.13
J4	151	0.790	141	1.05	0.72±0.14

c) Maximum Temperatures

It is clearly desirable to relate the flux density measurements to the surface temperature. To do so, it is necessary to assume a temperature distribution over the surface. Since for all practical purposes the subsolar point coincides with the subearth point, we shall use the coordinate system defined previously, i.e. z-axis toward the Sun and x-z plane passing through the Earth. One of the results from the eclipse photometry is that the surfaces of the Galilean satellites are even more insulating than the lunar surface. For a planet with little or no atmosphere, this implies that the maximum surface temperature occurs close to the subsolar point. We shall therefore assume the surface temperature distribution to be given by

$$T(\theta) = \left\{ \begin{array}{ll} T_{max}[\omega + (1-\omega)\cos^{\frac{1}{4}}\theta] & \theta \leq \pi/2 \\ T_{max}\omega & \theta \geq \pi/2 \end{array} \right\} \qquad (29)$$

where ω is the ratio of the dark side and limb temperature to T_{max}. We have also assumed axial symmetry about the z-axis. Equatorial and polar temperature-scans have been obtained at full Moon by Saari and Shorthill (1967). Their data, as reported by Bastin and Gough (1969), are shown in Figure 9 together with the assumed temperature distribution for ω = 0.3, 0.4, and 0.5. Again using the fact that the satellite surfaces are more insulating than the lunar surface, we have chosen ω = 0.3 to represent the Galilean satellites. We shall show, however, that the determination of T_{max} depends only weakly on the choice of ω. Note that the lunar data include the infrared phase function, i.e. the directivity of the emissivity for the Moon. We therefore need not account for the directivity of the satellite emissivities in this context if we assume that they are roughly equivalent to the Moon's.

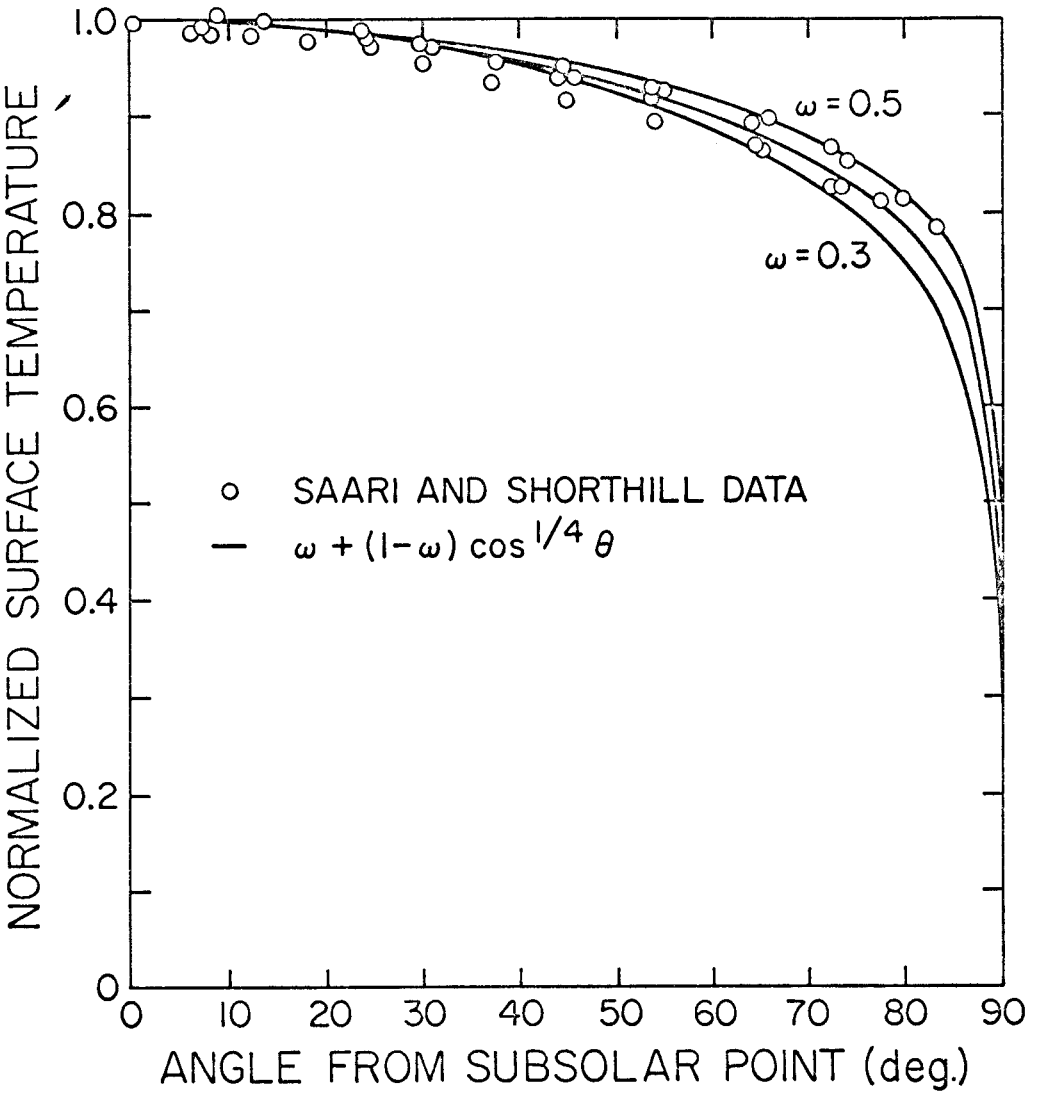

Fig. 9. - Polar and equatorial temperature scans at full Moon. Data from Saari and Shorthill (1967).

Finally, we assume that the 10μ emissivity, ϵ_{10}, is equal to 0.95. The maximum temperature is then given by a numerical evaluation of the equation

$$F_{10} = \frac{2\epsilon_{10} R^2 \pi}{D^2} \int_0^{\pi/2} \frac{B[10.16\mu,\ T(\theta)]}{C[T(\theta)]} \cos\theta \sin\theta \, d\theta \quad . \tag{30}$$

The results are listed in Table 9. To place limits on the uncertainty in T_{max}, we consider 4 sources of error:

(i) ω : $\frac{\partial T}{\partial \omega} \approx -8.5°K$, $\Delta\omega = 0.2 \rightarrow \Delta T = -1.7°K$

(ii) F_{10} : $\frac{\partial T}{\partial F} \approx \frac{\lambda T^2}{\gamma F}$, $\frac{\Delta F}{F} = 20\% \rightarrow \Delta T = 3°K$

(iii) R : $\frac{\partial T}{\partial R} \approx \frac{-2\lambda T^2}{\gamma R}$, $\frac{\Delta R}{R} = 10\% \rightarrow \Delta T = -3°K$

(iv) ϵ_{10} : $\frac{\partial T}{\partial \epsilon} \approx \frac{-\lambda T^2}{\gamma \epsilon}$, $\frac{\Delta \epsilon}{\epsilon} = 10\% \rightarrow \Delta T = 1.5°K$

In these expressions $\gamma = hc/k = 14413\mu°K$. If these uncertainties are assumed to be random, the expected uncertainty in T_{max} is less than 5°K.

TABLE 9

MAXIMUM SURFACE TEMPERATURES

	J1	J2	J3	J4
T_{max}(°K)	146 ± 5	136 ± 5	150 ± 5	161 ± 5

d) Bolometric Bond Albedo and Phase Integral

In order to estimate the bolometric Bond albedo, further assumptions are necessary:

(i) The satellite surfaces are assumed to be in thermal equilibrium.

i.e. the energy radiated away by the entire sphere is equal to the energy absorbed by the sphere.

(ii) The energy received from Jupiter is assumed negligible compared to the energy received from the Sun. Were it not for eclipses, the side of J1 which faces Jupiter could receive as much as 10% more energy than the other side due to Jovian thermal radiation and reflected sunlight. The effect is largely cancelled out, however, because the Jupiter-side of J1 is preferentially deprived of solar energy during eclipse.

Under these assumptions, the bolometric Bond albedo is given by

$$\pi R^2(1 - A_{bol})\, S_\odot = 2\pi R^2 \int_0^\pi \left\{ \int_0^\infty \epsilon(\lambda)\pi P[\lambda, T(\theta)]\, d\lambda \right\} \sin\theta\, d\theta \qquad (31)$$

where $S_\odot$ is the insolation evaluated at Jupiter's distance from the Sun, and $P[\lambda, T(\theta)]$ is the Planck function. Measurements of $S_\odot$ at 1 a.u. have recently been reviewed by Labs and Neckel (1971) who prefer $S_\odot$(1 a.u.) = 1.95 cal/cm^2 min.

Because the emissivity depends on wavelength, we cannot use $\epsilon\sigma T^4(\theta)$ for the wavelength integral. Instead 2 models, shown in Figure 10, have been investigated. Both models are consistent with the previously deduced emissivity ratio. In addition to these two models, A_{bol} has been calculated for a wavelength independent emissivity for comparison purposes. This last model is, however, not consistent with the observed emissivity ratio.

Since $A_{bol} = p_{eff}\, q_{eff}$, as already discussed, one obtains an estimate of q_{eff} for each value of A_{bol} calculated. Table 10 lists results from the 3 emissivity models. The uncertainty given behind each value corresponds to a temperature uncertainty of $\mp$ 5°K.

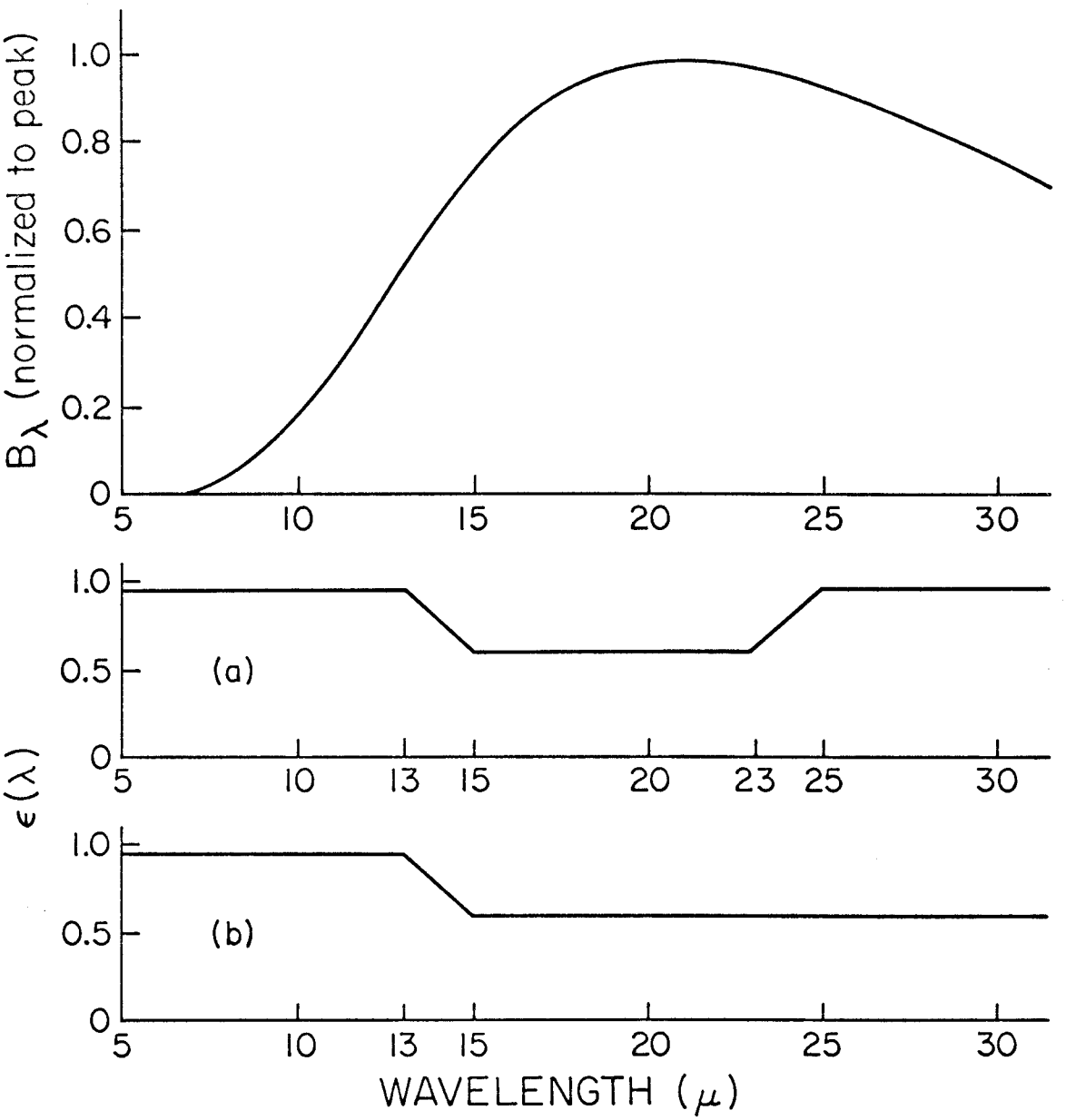

Fig. 10. - Emissivity models. Top: Planck function, B_λ, for a 140° K source. (a): Model (a), $\epsilon_{10} = 0.95$, dip adjusted to ϵ_{20} for each satellite. (b): Model (b), $\epsilon_{10} = 0.95$, $\epsilon(\lambda) = \epsilon_{20}$ $\lambda > 15\mu$. Model (c), not shown, has $\epsilon_{20} = \epsilon_{10} = 0.95$. Model (c) is inconsistent with the measured $\epsilon_{20}/\epsilon_{10}$ ratio.

TABLE 10

BOLOMETRIC BOND ALBEDOS AND EFFECTIVE PHASE INTEGRALS

Object		Model(a)		Model(b)		Model(c)	
	p_{eff}	A_{bol}	q_{eff}	A_{bol}	q_{eff}	A_{bol}	q_{eff}
J1	0.56	0.47±0.08	0.84±0.13	0.63±0.05	1.11±0.10	0.41±0.09	0.72±0.15
J2	0.69	0.60±0.06	0.87±0.09	0.71±0.15	1.03±0.07	0.56±0.07	0.81±0.10
J3	0.40	0.41±0.09	1.02±0.22	0.54±0.07	1.35±0.17	0.35±0.09	0.88±0.24
J4	0.17	0.20±0.11	1.2 ±0.6*	0.33±0.09	1.9 ±0.5	0.13±0.11	0.8 ±0.6

*From other considerations, the lower limit appears more plausible.

We note the following

(i) The two "realistic" models, (a) and (b), both yield values for the effective phase integral which are considerably higher than the phase integrals of the Moon (0.585) and Mercury (0.563), (Harris, 1961).

(ii) Even if the 20μ emissivity were not lower than that at 10μ, one still obtains phase integrals which are greater than those of the Moon and Mercury (Model c).

(iii) The uncertainty inherent in the determination of q_{eff} for J4 is so large, due to J4's low geometric albedo, that the calculation appears useless. However, J4 is the hottest of the satellites and the assumed 5°K temperature uncertainty is probably too conservative.

e) Summary

The main results from this study, applicable to each of the Galilean satellites, are the following:

(i) the mean flux densities in the 10 and 20μ band passes have been obtained, and the brightness temperatures have been calculated.

(ii) the effective 20μ emissivity has been shown to be significantly less

than the effective 10μ emissivity.

(iii) the maximum temperature has been calculated.

(iv) the bolometric Bond albedo has been indirectly determined, and

(v) the effective phase integral has been estimated, and shown to be greater than the phase integral of either the Moon or Mercury.

A discussion of the implications of these results will be deferred until the eclipse data have been presented.

IV. ECLIPSES

a) Introduction

In 1971 Jupiter's satellite plane was oriented relative to its orbit plane in such a way that Io (J1), Europa (J2), and Ganymede (J3) passed through Jupiter's shadow once every orbit. These events are referred to as "eclipses of the Galilean satellites". They should not be confused with occulations, in which Jupiter blocks the line of sight between the satellite and the Earth. Both events are characterized by the satellite becoming invisible to an observer on Earth, but there the similarity stops. During an eclipse, which lasts about 2 hours for each of the satellites, the satellite is denied solar energy with two predictable results: (i) the reflected light drops to zero, and (ii) the surface cools down due to radiation losses. Figure II depicts an eclipse of J3. For J1 and J2 the two events always merge in the following sense: Before Jupiter's opposition J1 and J2 are seen to dissappear into eclipse and reappear from occultation, and after Jupiter's opposition they are seen to disappear into occultation and reappear from eclipse. In other words, it is impossible to follow J1 and J2 completely through an eclipse.

Eclipses of satellites with little or no atmosphere offer an ideal opportunity for remote determination of various surface properties. To be more specific, infrared flux measurements at wavelengths long enough to measure predominantly thermal emission are indicative of the thermal conductivity and heat capacity of the upper soil layer, when obtained during or shortly after eclipse. For that reason, eclipses of the Moon have been measured and interpreted by several observers. Interpretation of lunar eclipses is complicated by two factors which, we shall see, do not significantly affect the interpretation of the Galilean satellite eclipses. The first of these is the

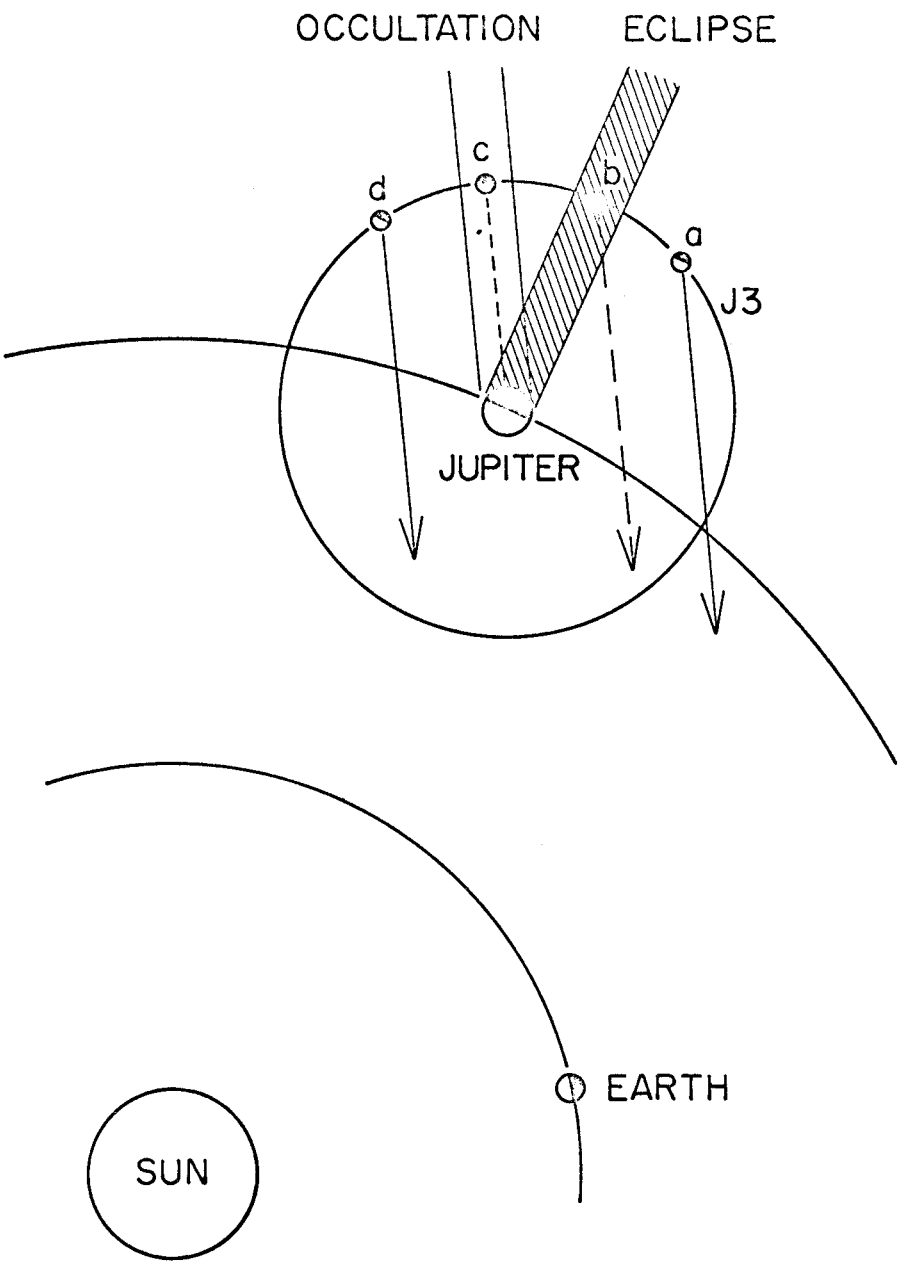

Fig. 11. - Eclipse configuration of J3 before Jupiter's opposition. J1 and J2 are so close to Jupiter that eclipses merge into occultations and vice versa (after opposition). Scale distorted.

high lunar daytime surface temperature (ca. 350°K). It turns out that the thermal parameters used in the interpretation of eclipse phenomena become severely temperature dependent above ≈200°K. This fact has caused serious misinterpretations of lunar eclipses which only recently have been corrected. The reader is directed to Winter and Saari (1969) and Linsky (1966). The second factor is the length of the penumbral period. For the Moon that period is about 60 minutes, whereas for the Galilean satellites it is less than 13 minutes. In the latter case, the brevity of the penumbral period enables us to make certain assumptions that are not valid for lunar eclipses. These assumptions will be discussed in context.

The infrared flux from Jupiter's satellite Ganymede (J3) has been measured during eclipse by Murray, Westphal and Wildey (1965). They were able to measure the cooling and subsequent heating rate, but could not detect the satellite during the intermediate period of the eclipse. From the observed rates they were able to conclude that J3 was essentially without an atmosphere and that its surface consisted of particulate material (low thermal conductivity). The measurement was repeated recently at 20μ with somewhat better signal to noise ratio by Morrison et al. (1971). Because of improved sensitivity and the use of a longer wavelength, these authors were able to record measurements right through the eclipse of J3, and saw the flux level drop to about 15% of maximum intensity by the end of the eclipse. By fitting their data with a homogeneous model (thermal models will be discussed later) they obtained a best fit for $\gamma = (k\rho c)^{-\frac{1}{2}} = 1400 \pm 500$ cm^2 °K sec$^{\frac{1}{2}}$/cal, where "k" is the thermal conductivity, and "ρ" the density and "c" the specific heat. The homogeneous model did not adequately account

for the high heating and cooling rates observed, however, and the authors (Morrison, 1972) are considering a more sophisticated model.

In view of the interesting nature of the visible light eclipse photometry of J1 and J2, it is, however, these two satellites that promise to be most rewarding for infrared investigation. It was therefore decided to give top priority to eclipses of J1 in this work.

As a result of this investigation, we shall show (1) that the surface materials of J1, J2, and J3 are particulate, (2) that any atmosphere present on either J1, J2 or J3 must have a surface pressure less than 1 mbar, (3) that a homogeneous thermal model cannot account for the observed heating rates of the satellites, and (4) that the surface material on J1 differs fundamentally from that on either J2 or J3.

b) Eclipse Data

(i) Measurements

All the eclipse data used in this work were obtained in 1971 between June 17 and September 20. The opposition of Jupiter occurred on May 23, placing all the observations after opposition. This means that only reappearances of J1 and J2 could be observed. That is not a serious drawback, however, because all the available information is contained in that part of the eclipse. Because of the geometry, J3 could be seen to enter and leave eclipse on both sides of opposition. Attempts were made to measure every available eclipse, but, because of weather conditions and other difficulties, only 10 satisfactory data sets, all at 10μ, were obtained . The relevant observational data are listed in Table 11.

Measurements were made using the same double beam sky subtraction

TABLE 11

DATES OF ECLIPSE OBSERVATIONS

Satellite	Event	1971 Date	Telescope	Aperture Diameter
1	Ec.R.	June 17	100in. M.W.	7.5"
1	Ec.R.	July 2	200in. P.M.	7.5
3	Ec.D.	July 3	200in. P.M.	5
1	Ec.R.	July 4	200in. P.M.	5
1	Ec.R.	July 11	60in. M.W.	10
1	Ec.R.	July 27	200in. P.M.	5
3	Ec.D.	Aug. 15	200in. P.M.	5
1	Ec.R.	Sept. 4	200in. P.M.	5
1	Ec.R.	Sept. 11	200in. P.M.	5
2	Ec.R.	Sept. 17	200in. P.M.	5

Ec.R.: eclipse reappearance, Ec.D.: eclipse disappearance, M.W.: Mt. Wilson, P.M.: Palomar Mountain.

technique described earlier. In the case of eclipses, however, the object was not moved from beam to beam due to the proximity of Jupiter. Instead, deflections were made by alternating between having both beams on the sky and one beam on the satellite with the other on the sky. Contamination from Jupiter was a suspected source of error. Figure 12 shows Jupiter, the three satellites during times of observation, and the beam size most frequently used for the measurements. To check contamination from Jupiter the sky was measured alternately to the east, west and south. No significant difference was observed for the three positions, and it was concluded that contamination from Jupiter was not an important source of error.

Perhaps the greatest advantage of using the 200 inch telescope for this kind of measurement was the ability to locate and measure J1 prior to reappearance. On three occasions it was possible to measure the flux before the satellite was again heated.

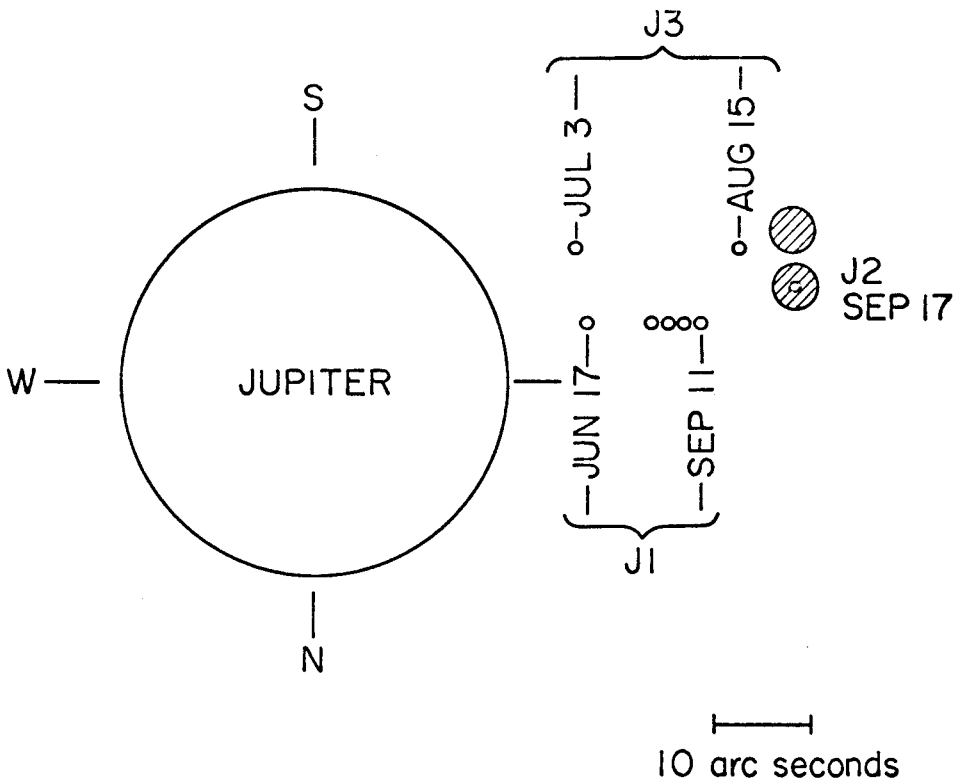

Fig. 12. - Positions of the satellites at various eclipse dates. The aperture size and spacing used on the 200 inch telescope is indicated. Approximately to scale.

(ii) Data Reduction

To improve the signal to noise ratio, all the data sets for each satellite have been separately normalized, combined into one set, and then smoothed with a "Gaussian filter" with $\sigma = 0.8$ min. as follows. An average point was derived for every two minutes along the time axis by weighting data points according to

$$w = e^{-t^2/2\sigma^2} \tag{32}$$

where "w" is the weight assigned to a data point aquired at time "t" relative to the time for the average point. To count each data point equally requires that

$$\int_0^{\Delta t/2} (1-e^{-t^2/2\sigma^2})\,dt = \int_{\Delta t/2}^{\infty} e^{-t^2/2\sigma^2}\,dt \quad . \tag{33}$$

For $\Delta t = 2$ min., $\sigma = \Delta t/\sqrt{2\pi} \approx 0.8$ min.

Error bars may be assigned to the averaged points by analogy between the Gaussian filter and a "square box filter", i.e. the standard deviation of the averaged point is taken to be

$$s = \left(\frac{\sum (F - f_i)^2 w_i}{\sum w_i}\right)^{\frac{1}{2}} \Bigg/ \left(\sum w_i\right)^{\frac{1}{2}} \tag{34}$$

in the Gaussian case, instead of

$$s = \left(\frac{\sum (F - f_i)^2}{N}\right)^{\frac{1}{2}} \Bigg/ \sqrt{N} \tag{35}$$

in the "square box" case. In equations 34 and 35, F is the average point, and f_i is the i'th datum contributing to F.

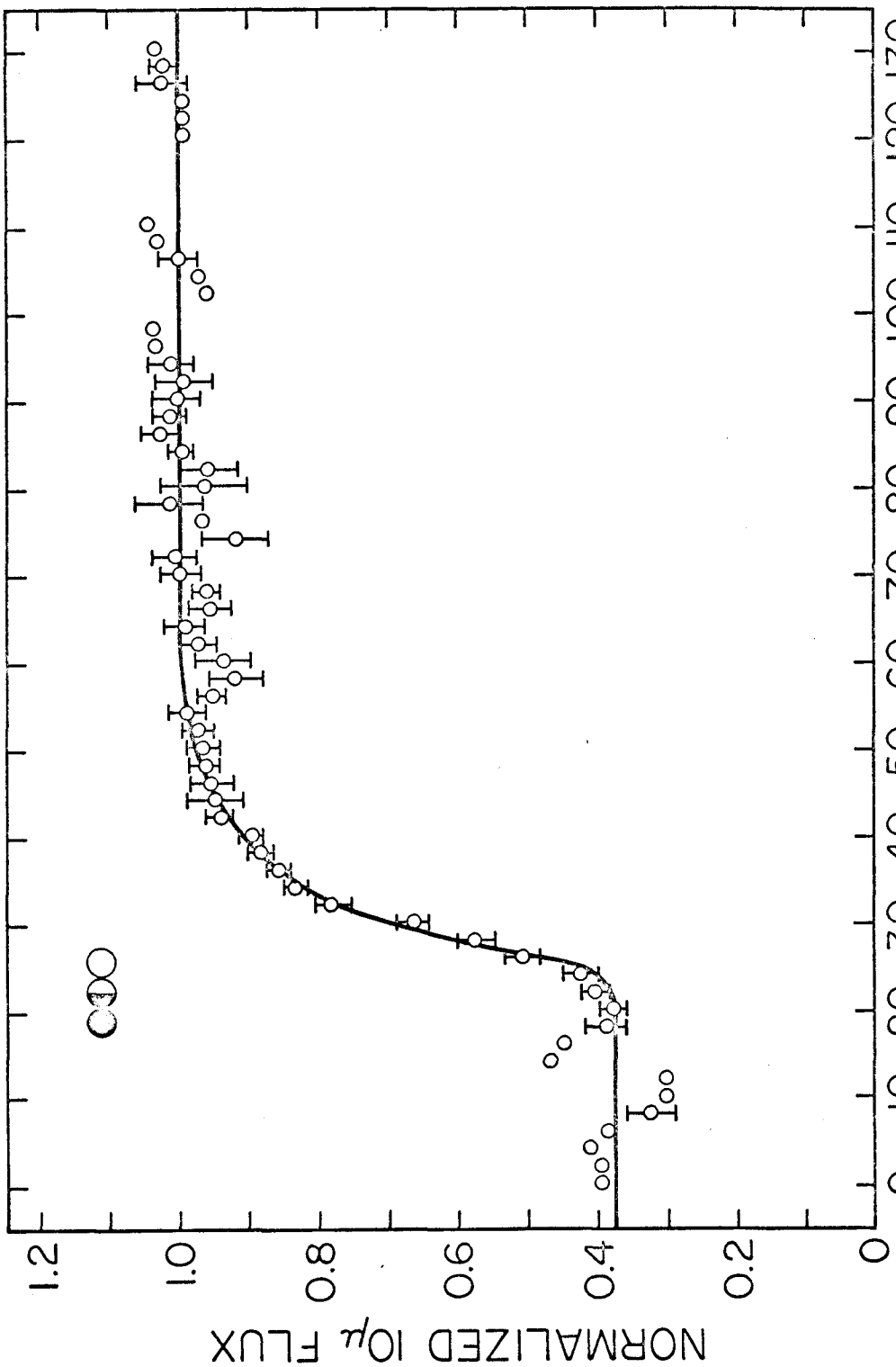

Fig. 13. - Eclipse heating data for J1 in 10μ. bandpass. Missing error bars indicate that only one data point within the pertinent two minute averaging period was obtained. Continuous curve is best fit from the two-layer model.

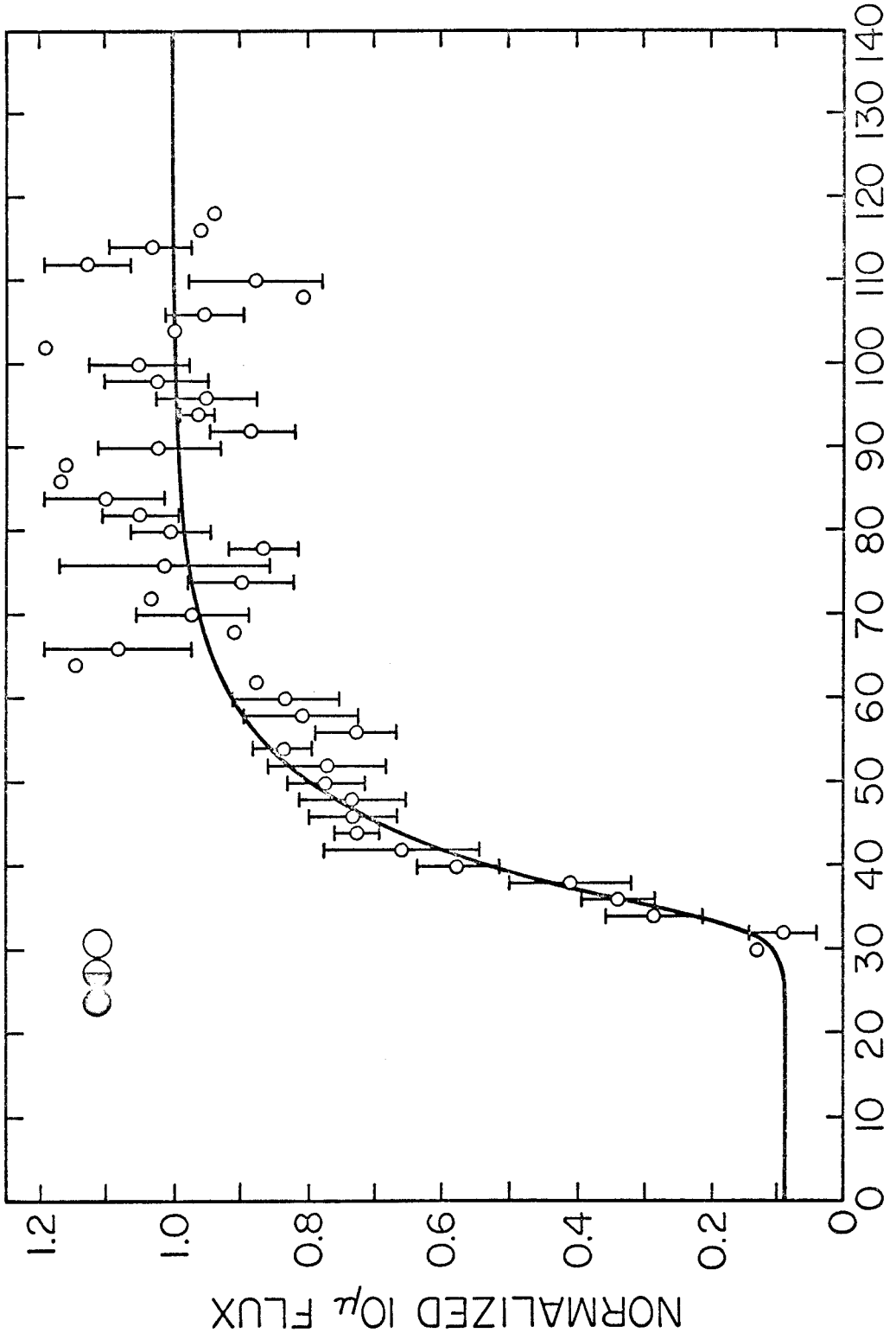

Fig. 14. - Eclipse heating data for J2 in 10μ bandpass. Missing error bars indicate that only one data point within the pertinent two minute averaging period was obtained. Continuous curve is best fit from the two-layer model.

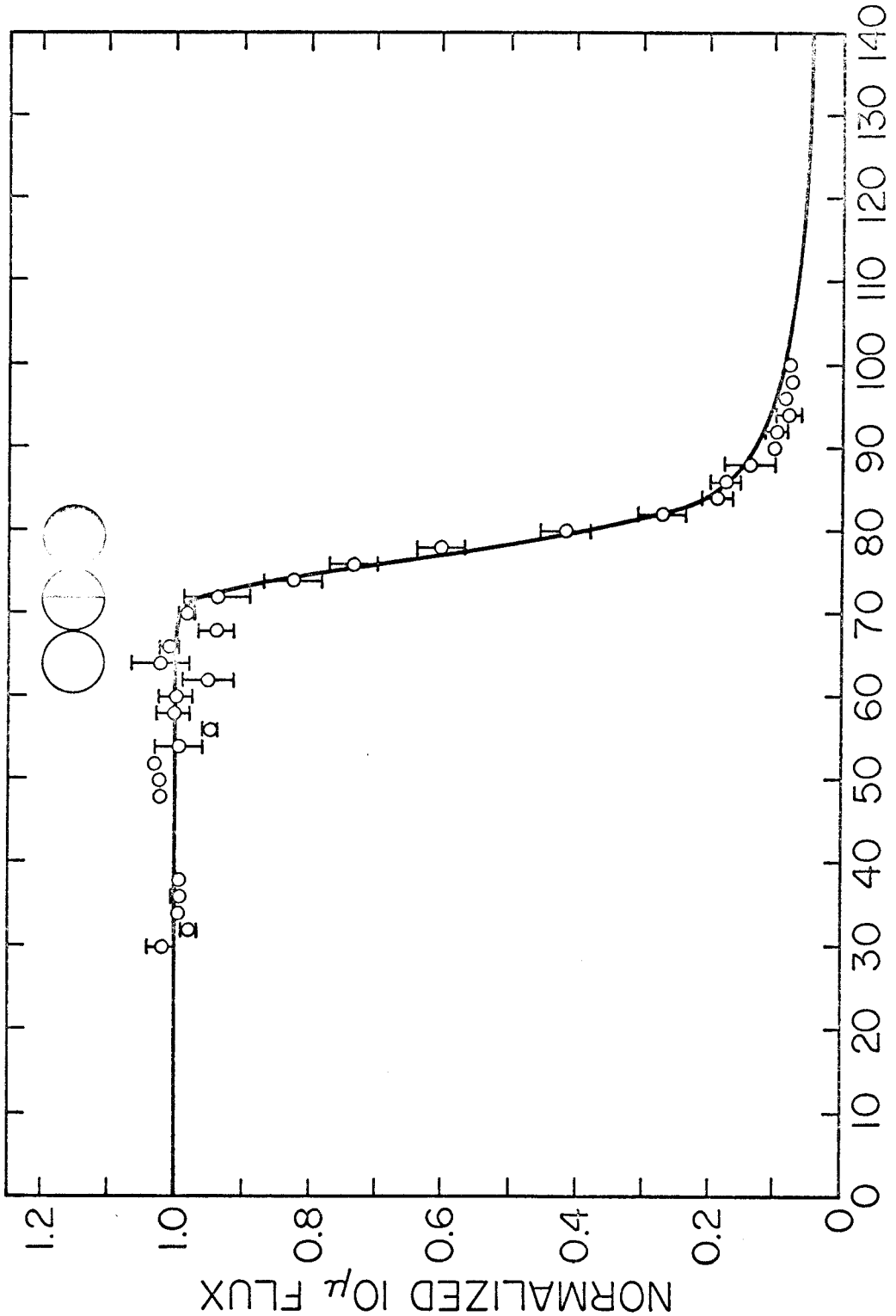

Fig. 15. - Eclipse cooling data for J3 in 10μ bandpass. Missing error bars indicate that only one data point within the pertinent two minute averaging period was obtained. Continuous curve is best fit from the two layer model.

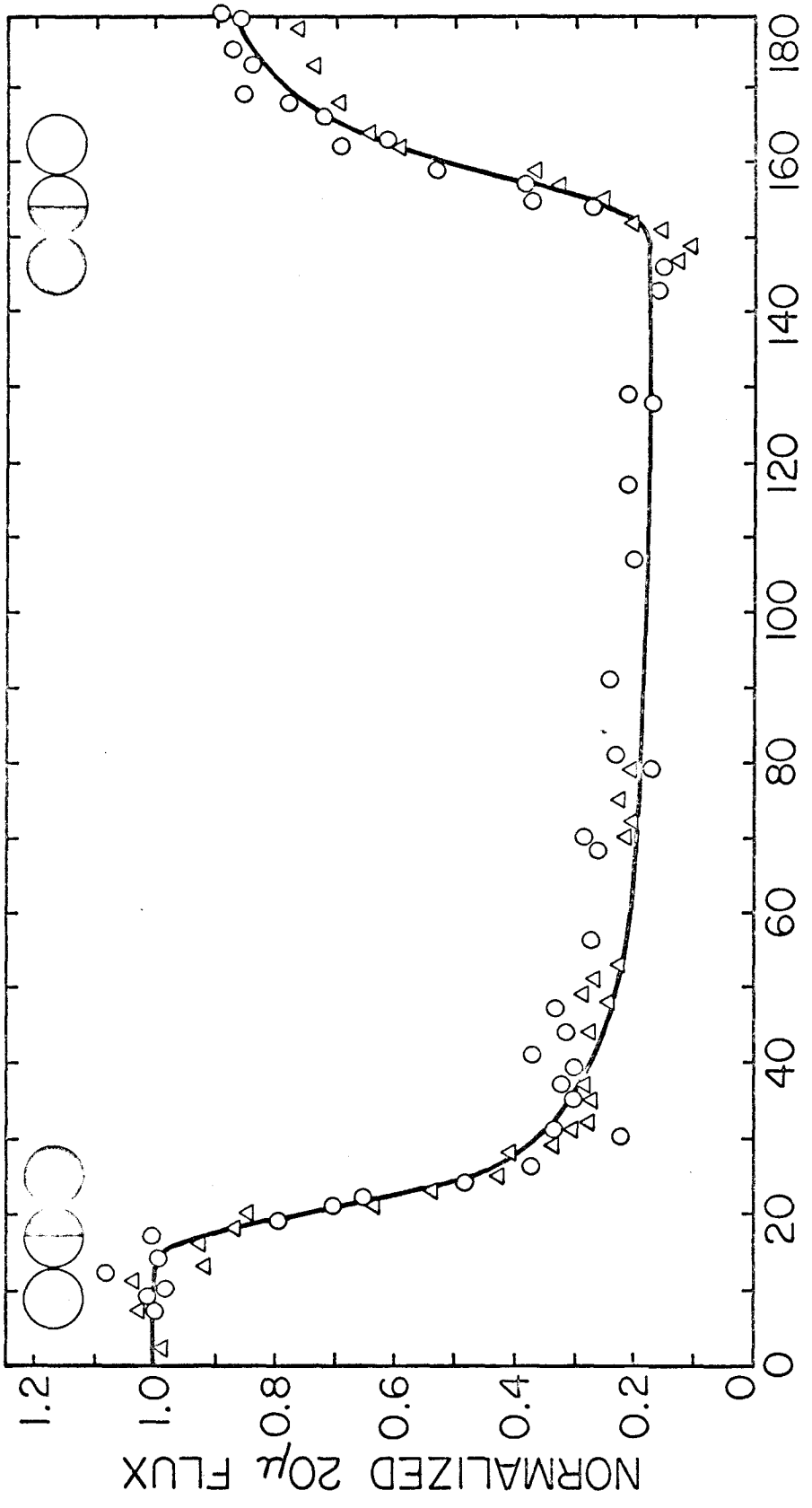

Fig. 16. - Eclipse cooling and heating data for J3 in 20μ bandpass, from Morrison et al. (1972). Data points shown as triangles were obtained before the opposition of Jupiter. Points shown as circles were obtained after opposition. Continuous curve is best fit from two-layer model.

The averaged points, with total error bars equal to twice the standard deviation, are plotted in Figures 13 through 15. The continuous curves will be discussed later.

The only assumptions going into the smoothing process is that there are no high frequency variations in the satellite temperatures, and that systematic differences between separate data sets are negligible compared to the noise within any given data set. The first assumption clearly holds from physical considerations. The second has been justified by comparing the averaged points to each data set by itself and verifying that the individual set was compatible with the averaged points.

c) Thermal Models

(i) Mathematical Formulation

Laboratory measurements of the thermal conductivity, k, and the heat capacity, ρc, will be reviewed in the next section. It will be shown that these parameters may, to a good approximation, be treated as constants at temperatures lower than 150°K. The thermal problem therefore reduces to solving the heat diffusion equation in a semi-infinite solid with constant parameters. For bodies much larger than the thermal skin depth, as is certainly the case with a natural satellite, the problem reduces to one dimension (Wessellink, 1948). Assuming that internal heat sources are negligible, the equations are

$$\epsilon \sigma T^4(o,t) = (1 - A)\, S_{\odot} \times f(t) + k \frac{\partial T(x,t)}{\partial x} \Bigg|_{x = o} \qquad (36a)$$

$$\rho c \frac{\partial T(x,t)}{\partial t} = k \frac{\partial^2 T(x,t)}{\partial x^2} \qquad (36b)$$

$$T(x \rightarrow \infty, t) = \text{constant} \qquad (36c)$$

where ϵ, σ, A, $S_\odot$ are the emissivity, Stefan-Boltzmann constant, bolometric Bond albedo, and solar flux at Jupiter defined in Part III, and T(x,t) is the temperature at time "t" a depth "x" below the surface. Because k and ρc are assumed to be constants, they may be combined into a single constant $\gamma = (k\rho c)^{-\frac{1}{2}}$ by scaling the depth parameter. Let $z = x/k$, then

$$\frac{\partial T(x,t)}{\partial x} = \frac{1}{k}\frac{\partial T(z,t)}{\partial z} \quad \text{and} \quad \frac{\partial^2 T(x,t)}{\partial x^2} = \frac{1}{k^2}\frac{\partial^2 T(z,t)}{\partial z^2} \ .$$

Hence

$$\epsilon\sigma T^4(o,t) = (1 - A)S_\odot \times f(t) + \frac{\partial T(z,t)}{\partial z}\Bigg|\ z = o \qquad (37a)$$

$$\frac{\partial T(z,t)}{\partial t} = \gamma^2 \frac{\partial^2 T(z,t)}{\partial z^2} \qquad (37b)$$

$$T(z \to \infty, t) = \text{constant} \qquad (37c)$$

The second equation set may be solved by implicit numerical techniques for various choices of γ. The technique employed in this work was taken from Burnett (1971) and modified to suit the problem at hand. A brief description of the numerical technique is given in Appendix (a).

(ii) Model Assumptions

To reduce computing cost, the following assumptions have been made: (1) that the satellite may be treated as a flat disk facing the sun, (2) that the eclipse occurs simultaneously over the entire disk, (3) that the temperature is uniform with depth prior to eclipse, and (4) that the gradual decrease and increase of the insolation is adequately described by

$$f(t^*) = \cos^2\left(\frac{\pi}{2} \times \frac{t^*}{t_{pen}}\right) \qquad (38)$$

where t_{pen} is the penumbral period and t* is either the time from the start of the eclipse ($o \leq t^* \leq t_{pen}$) or the time before the end of the eclipse ($t_{pen} \leq t^* \leq t_{end}$).

The first 2 assumptions have been tested and found to hold extremely well, provided an "effective temperature", similar to the brightness temperature, is used in the calculations. The test results are discussed in Appendix (b). The third assumption is based on the rapid return ($\approx$20 min.) to normal surface temperature following an eclipse, evident in the data. The last assumption has been tailored to the visible eclipse photometry, which is an excellent measure of the gradual extinction of the insolation. The sources for the visible photometry are: J1 (Franz and Millis, 1970) t_{pen} = 3 min., J2 (Greene, Shorthill, and Despain, 1971) t_{pen} = 6.5 min., and J3 (Price and Hall, 1971) t_{pen} = 13 min.

d) Results

(i) Homogeneous Model

Eclipse curves have been calculated from the homogeneous model for a wide range of γ-values. Attempts to fit the J1 eclipse data are shown in Figure 17. The dashed curve in the figure corresponds to the data. Referring to Figure 17 the following important points can be seen. (1) For γ-values less than 40**, typical of solid rock or dense ice, no appreciable cooling takes place during the eclipse. We may therefore conclude that J1 does not have a solid rock or ice surface. (2) The flux level just prior to reappearance can be predicted from the model with $\gamma \approx 500$, a value

---

**Here and elsewhere, γ is given in units of $^{\circ}K\ cm^2\ sec^{\frac{1}{2}}/cal$.

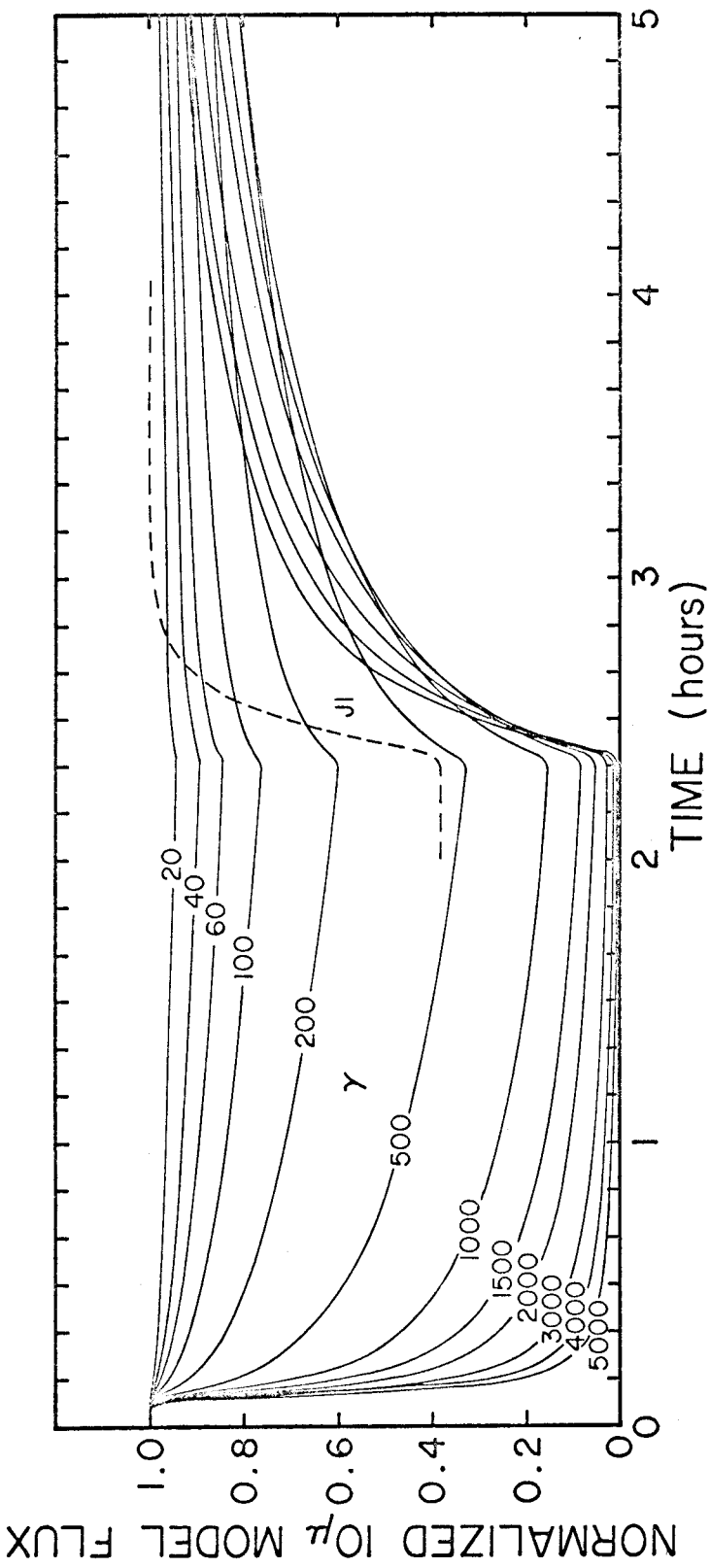

Fig. 17. - Eclipse curves generated from the homogeneous model with $\gamma = 20 \rightarrow 5000\,^{\circ}\mathrm{K\,cm^2\,sec^{\frac{1}{2}}/cal}$. Dashed curve represents J1 10μ data.

corresponding to porous rock in vacuum. However, the predicted heating rate with such a γ-value is much lower than that observed, so we have to go to considerably higher γ-values. (3) As γ is increased the predicted heating rate approaches that observed, but the predicted flux level prior to reappearance falls below the observed level. In fact, there exists no value of γ for which the homogeneous model predicts the observed eclipse curve.

(ii) Model With Lateral Inhomogeneity

To modify the homogeneous model, one can introduce lateral or vertical inhomogeneity. For the first type, we note that the observed heating rate requires a very high γ for one component of the surface material. That component will exibit a near zero flux level prior to reappearance. Therefore the second component, assuming a two-component system, must have a low γ ($\approx$20), and cover a fraction of the area roughly equal to the flux fraction observed just prior to reappearance. For J1 this fraction amounts to having $\approx$35% of the surface covered with the low-γ component. Since virtually no cooling of that material takes place, we may simply add a constant ($\approx$0.35) to any of the high-γ curves, and renormalize the result. Again one fails to find a γ-value for which the model predicts a return to normal surface temperature in 15-20 minutes, as observed, without overshooting the initial heating rate. We conclude that lateral inhomogeneities are inadequate to explain the observed eclipse curve.

(iii) Two-Layer Model

The next simplest model involves a vertical inhomogeneity in the form of a two-layer structure. The top layer must respond quickly to the insolation; therefore its γ-value will be high. Yet, it must not cool too much during

the eclipse; hence it must be supplied with energy from the lower layer at a significant rate. For energy to reach the surface through a low conductivity (high γ) layer, that layer must be thin. If the top layer is thin, the lower layer will cool, thus shutting off the energy supply, unless the conductivity in the lower layer is very high. We are therefore forced to the following model:

The surface of J1 consists of a thin upper layer with low thermal conductivity covering a subsurface with high (rock or ice-like) thermal conductivity.

For simplicity the preceeding statements were made in relation to J1. However, they apply equally well to J2 and J3. The two-layer model has therefore been investigated for all three satellites. From the homogeneous model, it is seen that "low γ-material" does not cool to any extent during the eclipse; the solution for the two-layer model was therefore simplified by holding the temperature at the bottom of the top layer fixed in time. A best fit, decided visually, to the eclipse data yields two parameters: the γ-value and the thickness, τ, of the top layer. No detailed information is obtained about the subsurface, other than its high thermal conductivity. Numerical values for the two-layer model parameters are listed in Table 12. In order to specify k and τ, it is necessary to assume a value for ρc. We have made a tentative choice of $\rho c = 0.45$ Joule/$^\circ$K cm^3, which will be explained later. For any other choice of ρc, the relationships are $k_2 = k_1 (\rho c)_1/(\rho c)_2$ and $\tau_2 = \tau_1 (\rho c)_1/(\rho c)_2$.

TABLE 12

SURFACE PARAMETERS DETERMINED FROM TWO-LAYER MODEL

Satellite	γ ($^\circ$K cm^{2}sec$^{\frac{1}{2}}$/cal)	$10^6 k$ (Watt/$^\circ$K cm)	τ (cm)
J1	1100 ± 100	32 ± 7	0.37 ± 0.06
J2	3000 ± 1000	4 ± 3	0.2 ± 0.1
J3	3400 ± 700	4 ± 1	0.22 ± 0.06

(iv) Limits of Uncertainty in γ, k, and τ

The limits of uncertainty shown after each γ, k, and τ in Table 12 were derived from the uncertainty in the data as follows.

It was found that the computed eclipse curves for the two-layer model could be characterized by two parameters: $A = k/\tau$, which governed the flux fractions just prior to reappearance, and $B = k/\tau^2$, which controlled the steepness of the heating curves. In particular, the computed flux fraction, h, and the time-lag* for heating, t, were found to be linear in A and B, i.e.

$$h = a + (dh/dA)A \tag{39}$$

$$t = b + (dt/dB)B \tag{40}$$

$$\Rightarrow \quad \Delta A = \left(\frac{1}{A}\frac{dA}{dh}\right)\frac{k}{\tau}\Delta h \equiv \alpha\frac{k}{\tau}\Delta h \tag{41}$$

$$\Delta B = \left(\frac{1}{B}\frac{dB}{dt}\right)\frac{k}{\tau^2}\Delta t \equiv -\beta\frac{k}{\tau^2}\Delta t \quad , \tag{42}$$

where Δh and Δt are the uncertainties in the observed flux fraction prior to

*The time-lag for heating was taken arbitrarily as the time between the end of the eclipse (first ray of sun) and the time when the flux level had reached 90% of maximum intensity.

reappearance, and the time-lag for heating respectively. It is easily shown that

$$\Delta k/k = 2\alpha\Delta h + \beta\Delta t \tag{43}$$

and

$$\Delta\tau/\tau = \alpha\Delta h + \beta\Delta t. \tag{44}$$

Also

$$\gamma = (k\rho c)^{-\frac{1}{2}} \Rightarrow \Delta\gamma/\gamma = -0.5\ \Delta k/k \quad . \tag{45}$$

The values of α and β, determined by varying A and B in the model, and the values of Δh and Δt, adopted by considering the uncertainty in the observational data, are listed in Table 13.

TABLE 13

UNCERTAINTY FACTORS FOR γ, k, τ

Satellite	Δh	Δt	α	$\beta(\text{min}^{-1})$
J1	0.02	2 min.	3.33	0.050
J2	0.05	6 "	6.67	0.033
J3	0.03	4 "	5.00	0.033

(v) Discussion

The eclipse curves, generated from the two-layer model using the parameters listed in Table 12, are plotted over the observational data in Figures 13 - 16.

The model parameters for J3, as well as their uncertainty factors, were not obtained from the 10μ eclipse photometry of this work. The 20μ data from Morrison (1972) were considered more suitable because they included the heating part of the eclipse curve. However, the 10μ flux curve, computed for the parameters obtained by fitting the 20μ data, is in excellent agreement with the 10μ observations (Figure 15).

We wish to stress two points:

1) The two-layer model has only 2 free parameters, γ and τ. Yet the agreement between the predicted and the measured eclipse curves is excellent throughout the observed portions of the eclipses. We consider this agreement as a strong indication that the two-layer model is essentially the correct representation of the satellite surfaces.

2) The γ-value of J1 is distinctly different from the γ-values of J2 and J3. We shall come back to that point after a discussion of laboratory measurements.

e) Comparison With Laboratory Data

(i) Preliminaries

In general both the conductivity, k, and the specific heat, c, are temperature dependent. The "effective" disk temperatures used in the model calculations were 134, 122, and 138°K for J1→J3. The corresponding temperature decrease during eclipse, as deduced from the observed flux ratios were 13, 24, and 29°K. While the effective temperatures do not apply to the entire surface, the "mean" temperature drops can be taken as representative of the actual temperature variation. For simplicity, we shall therefore consider a temperature range of $110 \leq T \leq 150$°K in the following discussion.

(ii) Specific Heats

Measurements of the specific heat of several rock materials including quartz, magnesium silicate, calcium feldspar, diabase, diorite, granite, basalt, and silica glass have been reviewed by Winter and Saari (1969). They find that

$$c(T) = -0.034\ T^{\frac{1}{2}} + 0.008\ T - 0.0002\ T^{\frac{3}{2}} \quad , \tag{46}$$

where T is in °K and c(T) is in Joule/°Kgm, adequately describes all the

available data. For water ice, the Handbook of Physics and Chemistry gives

$$c(T) = 0.18 + 0.0069\,T \quad . \tag{47}$$

Thus, for the relevant temperature range, we have

$$c(130 \pm 20^\circ K) = 0.36 \pm 0.06 \text{ Joule}/^\circ K\,gm \quad \text{(Rock)} \tag{48}$$

$$c(130 \pm 20^\circ K) = 1.08 \pm 0.14 \quad " \quad \text{(Water Ice)} \quad . \tag{49}$$

This temperature variation is so small that constant values may be adopted without introducing serious error.

(iii) Thermal Conductivities of Solids

Horai et al. (1970) have measured the thermal conductivity of two lunar rock types (A and C). For $T \cong 130^\circ K$ their results are

$$k(130 \pm 20^\circ K) = (1.3 \pm 0.1) \times 10^{-2} \frac{\text{Watt}}{\text{cm}^\circ K} \quad \text{(Type A)} \tag{50}$$

$$k(130 \pm 20^\circ K) = (0.6 \pm 0.05) \times 10^{-2} \quad " \quad \text{(Type C)} \tag{51}$$

These values are lower than the corresponding values for earth rocks by about a factor of two, presumably due to interstitial water in the latter. Highly porous rocks in vacuum have slightly lower thermal conductivity. Wechsler and Glaser (1965) have summarized measurements on rocks with porosities $\approx 0.2 - 0.5$, which have conductivities as low as 10^{-3} watt/cm°K. For solid water ice, Dean and Timmerhaus (1962) have measured the thermal conductivity to be

$$k(T) = 6.36/T \quad \frac{\text{Watt}}{\text{cm}^\circ K} \qquad 20 < T < 273^\circ K \tag{52}$$

or

$$k(130 \pm 20^\circ K) = (4.9 \mp 0.8) \times 10^{-2} \frac{\text{Watt}}{\text{cm}^\circ K} \quad . \quad \text{(Water Ice)} \tag{53}$$

(iv) Thermal Conductivities of Powders in Vacuum

According to Watson (1964), and other investigators, the thermal conductivity of a powder in vacuum may, to a good approximation, be written

$$k = k_c + k_r T^3 \tag{54}$$

where k_c represents the contact conductivity between the grains and $k_r T^3$ is the contribution to k due to radiation. The values of k_c and k_r vary from one material to another as well as with the particle size and density of the material. For the Moon, the term $k_r T^3$ is comparable to k_c and must be taken into account for a successful interpretation of the observed thermal behavior of the lunar surface (Winter and Saari, 1969). The Galilean satellites, however, are much colder than the Moon, with the result that $k_r T^3 \ll k_c$ for common materials. Consider the thermal conductivity expressed as

$$k = k_c \left(1 + \frac{k_r}{k_c} T^3\right) \tag{55}$$

and study the two relevant columns in Table 14. Note that, except for pumice powder and large glass beads, the term $1 + (k_r/k_c) T^3 \approx 1$ for $T < 150^\circ K$. The error involved in neglecting the $(k_r/k_c) T^3$ term is therefore small, and we may assume that k is independent of temperature for the Galilean satellites.

TABLE 14

THERMAL CONDUCTIVITY OF POWDERS IN VACUUM

Description	ρ	Size Range (μ)	$10^6 k_c$ (Watt/°Kcm)	$10^{13} k_r$ (Watt/°K⁴cm)	$1 + \frac{k_r}{k_c} T^3$ T = 300°K	$1 + \frac{k_r}{k_c} T^3$ T = 150°K	References
Glass	?	10-20	4.8	2.3	2.30	1.162	Merrill (1968)
Beads		38-53	4.4	4.5	3.75	1.346	"
.....		44-62	4.7	3.0	2.73	1.210	Wechsler & Simon (1966)
.....		88-125	3.2	8.5	8.2	1.898	Watson (1964)
.....		125-243	8.7	6.4	3.0	1.249	Merrill (1968)
.....		250-350	1.0	13.0	35	5.4	Watson (1964)
Quartz	1.00	0-10	25.0	3.0	1.32	1.041	Wechsler & Simon (1966)
Powder	1.34	44-74	33.5	4.2	1.35	1.042	Watson (1964)
Pumice	.82	10-37	5.1	3.1	2.65	1.20	Wechsler & Simon (1966)
Powder	.84	44-74	2.5	3.6	4.89	1.48	"
Basalt	1.36	10-37	21.-1600/T	.88	1.15	1.03	"
Powder	1.43	44-74	6.1	2.1	1.92	1.12	"
.....	.79	37-62	5.09	1.69	1.90	1.112	Fountain & West (1970)
.....	.88	"	6.50	1.67	1.69	1.087	"
.....	.98	"	5.95	1.72	1.78	1.097	"
.....	1.13	"	8.87	1.90	1.58	1.073	"
.....	1.30	"	12.37	2.43	1.53	1.066	"
.....	1.50	"	16.42	3.43	1.56	1.070	"
Lunar Dust...	1.3	?	16.3	1.36	1.23	1.028	Birkebak & Cremers (1970)

(v) Thermal Conductivity of Powders Under Ambient Gas Pressure

If a powder is immersed in a gas, its thermal conductivity is affected. According to data summarized by Wechsler and Glaser (1965), there are three quite sharply defined gas pressure regimes dictated by the mean free path of the gas molecules: a low pressure ($p < 0.1$ mbar) regime in which the thermal conductivity of the powder is independent of ambient gas pressure, a medium pressure (0.1 mbar $< p < 500$ mbar) regime in which the thermal conductivity of the powder is directly proportional to the gas pressure, increasing from the vacuum conductivity by a factor of 100-200, and a high pressure ($p > 500$ mbar) regime in which the thermal conductivity again is roughly independent of gas pressure.

(vi) Discussion

Since the thermal conductivities inferred for the upper layers of J1, J2, and J3 are as low as those of powders in vacuum (Tables 12 and 14), we conclude that the surface pressures on these three satellites are probably lower than 0.1 mbar, and almost certainly less than 1.0 mbar. It goes without saying that the amount of solid rock or ice present on the surfaces of either of the three satellites must be negligible.

The thermal conductivity data from Table 14 were evaluated at $T = 140^{\circ}K$ and plotted in Figure 18, as a function of powder density. Also shown in the figure is the loci of thermal conductivities of J1, J2, and J3 consistent with the inferred γ-values and the specific heat of rock and mineral powders. The lower limit on the soil density is taken from Hapke and Van Horn (1963) who experimented with "fairy castle" structures. They found that fine grained powders, laid down in a few centimeters thickness, were quite stable against

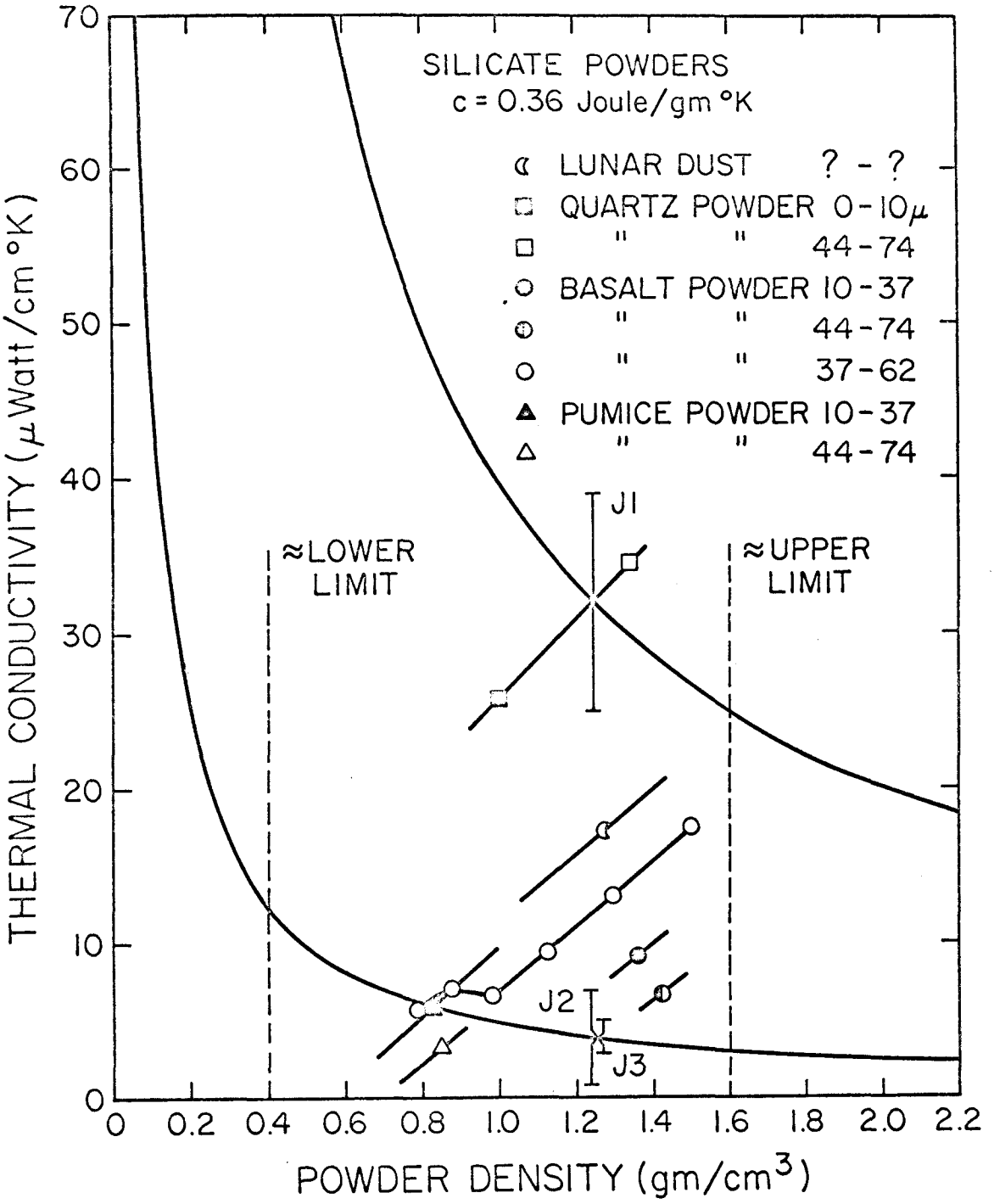

Fig. 18. - Loci of thermal conductivities consistent with the measured γ-values and specific heat = 0.36 Joule/gm °K. Experimental data from Table 14.

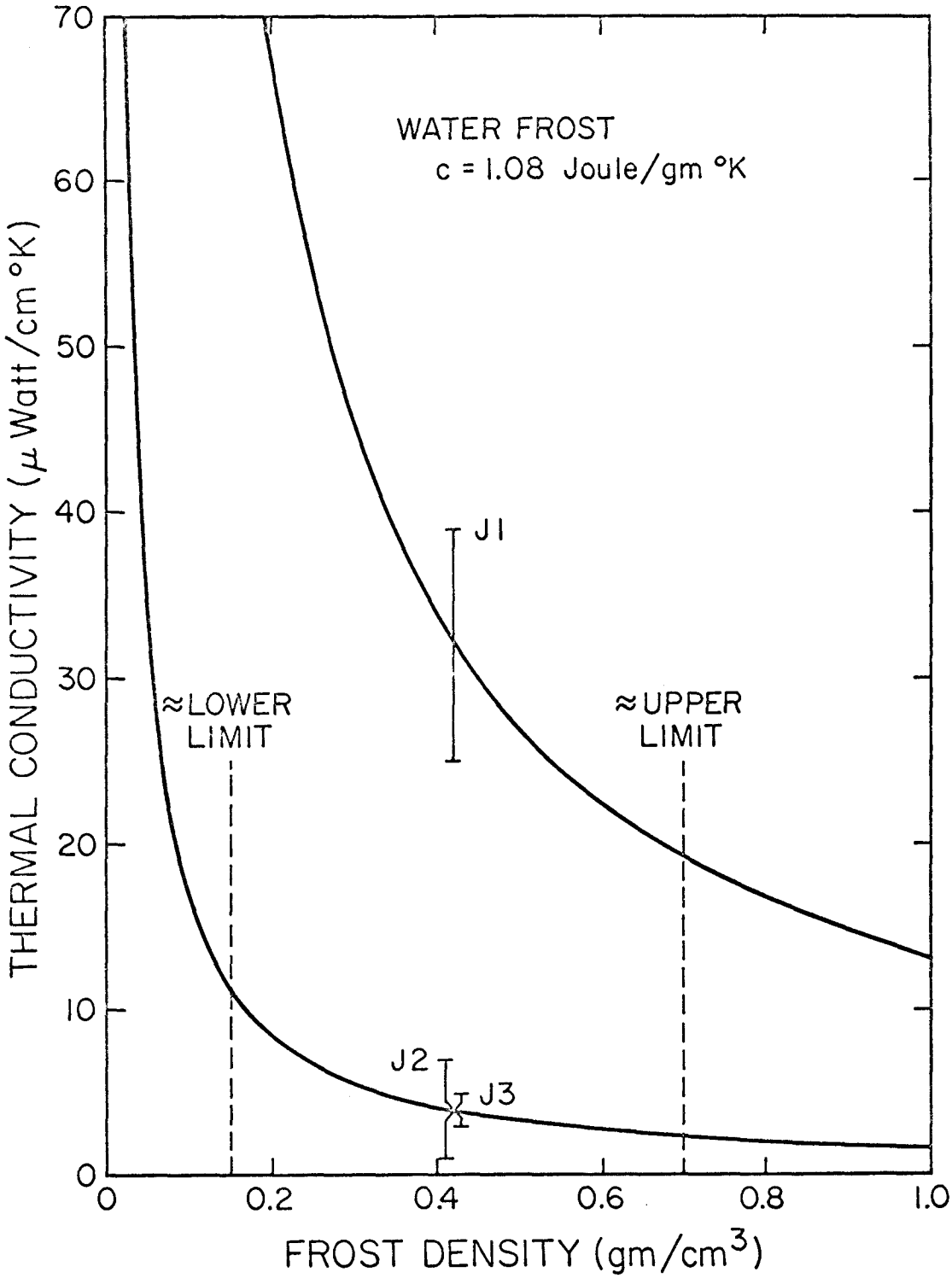

Fig. 19. - Loci of thermal conductivities consistent with the measured y-values and specific heat = 1.08 Joule/gm °K.

disruptive forces for densities as low as 10-20% of the solid-phase density. In accord with this result the lower soil density limit has been taken to be 15% x 2.7 gm/cm^3 $\approx$ 0.4 gm/cm^3. The upper limit to the soil density is difficult to ascertain, but must be somewhat less than the solid phase density. We would choose 1.6 gm/cm^3 as a plausible upper limit, but that limit does not affect the interpretation. The mean density of the powders appears to be about 1.25 gm/cm^3 leading to a heat capacity of 0.45 Joule/$^\circ$K cm^3. That is the value adopted to derive k and τ from γ for Table 12. Figure 19 is a plot for water frost similar to Figure 18 for silicate powders. We are not aware of laboratory data pertinent to this figure. Generalization to other frosts, by scaling the density axis, is obvious.

Referring to Figures 18 and 19, we have reached the conclusion that the surface material on J1 differs fundamentally from the materials on J2 and J3, as follows.

If J1 and J3* were covered with the same type of silicate powder, then either the particle size or the density of the powder must differ considerably between the two satellites. We should be able to investigate the first possiblity by comparing the emissivity ratio, $\epsilon_{20}/\epsilon_{10}$, of J1 to that of J3, since that ratio is affected by the particle size distribution. Because the emissivity ratios for J1 and J3 (Table 8) are nearly equal, it seems unlikely that the difference can be explained as a particle size effect. The second possibility requires that the powder density of the upper few millimeters of surface differs by a factor of $\approx$2 between J1 and J3. Such a porocity difference should lead to observable differences in the phase functions for small

*We consider J2 to be similar to J3.

phase angles (Oetking, 1966). However, the phase functions of J1 and J3 are virtually identical (Stebbins and Jacobsen, 1928). We therefore conclude that J1 and J3 are not covered by the same type of silicate powder. The same arguments can be applied to any other powder. In other words, J1 is covered by a powder type which is distinctly different from the powder types covering J2 and J3.

f) Conclusions From Part IV

1) The surface of J1, of J2, and of J3 consists of a thin (~mm) layer of thermally insulating, particulate material covering a subsurface with high (solid rock or ice-like) thermal conductivity.

2) The surface material on J2 appears to be similar to that of J3.

3) The surface material on J1 is significantly different from that of either J2 or J3.

4) The atmospheric surface pressures on J1, J2, and J3 are probably all less than 0.1 mbar, and almost certainly less than 1 mbar.

V. SUMMARY

The main results of this work are reconsidered below, in an attempt to form guidelines for future observations of the Galilean satellites, and restate the constraints on the range of possible surface materials.

a) Emissivity Ratio

The effective emissivity ratio, $\epsilon_{20}/\epsilon_{10}$, inferred from the 10 and 20μ brightness temperatures, is significantly less than unity for each of the four Galilean satellites. This result is difficult to reconcile with the fact that the surface materials on J1, J2 and J3 are particulate. Naturally occurring silicate powders (Griggs, 1968) and frosts (Keegan and Weidner, 1965) are expected to have infrared emissivities which are essentially independent of wavelength and colse to unity. A thorough examination of the possible causes of the low emissivity ratios is beyond the scope of this thesis. Two hypotheses have, however, been considered:

(1) The size distribution of the surface materials is very narrow compared to common terrestrial particulate materials.

It can be shown from Mie-scattering theory (Appendix c) that a powder, of which each particle has radius "a", exhibits a pronounced dip in its emissivity, ϵ (λ), at $\lambda \approx 2a$. Thus, if a significant fraction of the surface particles were about 10μ, a low 20μ emissivity should be expected.

(2) The surface material is very fine ($a < 3\mu$) silicate powder.

Hunt and Logan (1972) have shown that for small optically thin silicate particles, an emission maximum is produced in the reststrahlen region

($\approx 9\mu$). Their experiment was designed to measure the emissivity of an array of single particles, and does not necessarily relate to a three-dimensional surface. However, Conel (private communication) has found empirically that a loosely packed powder tends to emit very much like the predicted emission from an array of single particles.

There are presumably other ways to explain the low 20μ emissivity, including the previously mentioned directivity factor. It seems likely that the observed effect is real, however, and as such should be accounted for in any successful identification of the surface material on the Galilean satellites.

b) Maximum Surface Temperature

The maximum surface temperature, T_{max} has been determined for each satellite (Table 9). From T_{max} the approximate surface temperature, anywhere on the daytime hemisphere, may be derived from the assumed temperature distribution (Equation 29). These temperatures are more relevant than brightness temperatures to questions of the presence of volatiles and frosts. That is to say, the vapor pressure (which is to be compared to the upper limit on the surface pressure) of a volatile surface material is governed by the mean surface temperature, not by the brightness temperature. The theory of frost formation has recently been discussed by Veverka (1970), and shall not be reconsidered here.

c) Phase Integrals

The effective phase integrals of J1, J2 and J3 are nearly equal to 1.

The determination for J4 is too uncertain to warrant further consideration. Table 15 compares these values to directly measured phase integrals of the terrestrial planets.

TABLE 15

PHASE INTEGRALS OF THE TERRESTRIAL PLANETS AND THE GALILEAN SATELLITES

Planets	Phase Integral, q	Reference
Mercury	0.563	From Harris (1961)
Moon	0.583	"
Mars	1.04	"
Earth	1.095	"
Venus	1.296	"
J1	0.84 ± 0.13	Present Work
J2	0.87 ± 0.09	"
J3	1.02 ± 0.22	"
J4	1.2 ± 0.6*	"
Lambert Sphere	1.500	

Note that only planets with reflecting atmospheres have phase integrals as high as those of the Galilean satellites. Yet, we have shown the surface pressures on J1, J2, and J3 to be less than 1 mbar. For J1 the upper limit is 10^{-3} mbar (Taylor, et al 1972). It is doubtful that an atmosphere with a surface pressure less than 10^{-3} mbar could affect the reflectivity of J1. Since J1's q-value is similar to those of J2 and J3, there is little reason to suppose that atmospheric reflection plays a role in increasing the phase integral of either of these three satellites. We therefore look to the surface material for an explanation. It is believed (Hapke, 1963, and 1966) that the lunar phase function can be understood in terms of

*From other considerations, the lower limit appears more plausible.

the microstructure of the surface material. A planet covered with dark, high opacity, loosely packed material should have a phase function which decreases sharply from zero phase angle, and continues to decrease monotonically with increasing phase angle. If the decrease is great enough (Minnaert, 1961), such a phase function leads to a phase integral similar to that of the Moon or Mercury. The surface materials on J1, J2, and J3 are bright (Harris 1961, Johnson 1971) powders (this thesis) with low opacity (Veverka, 1971). In such material multiple scattering takes place, and one might expect a gentler decrease in the phase function with consequently larger phase integrals. According to Johnson (1971), the phase functions of J1, J2, and J3, measured out to $\alpha = \pm 12°$, do decrease more gently than the lunar phase function. In making the comparison the upsurge of the Moon's phase function for $\alpha < 2°$ (Van Diggelen, 1965) is ignored because of the difficulty in observing the Galilean satellites at phase angles less than that.

The indirect determination of a phase integral is important for two reasons. (1) For J1, J2, and J3 the inferred q-values support previous evidence that the surfaces are covered by a bright low-opacity material. (2) It has been conventional to assume that atmosphere-less bodies have q-values close to the Moon's q-value. We have shown that this assumption is false for J1, J2, and J3, and presumably for other bright satellites as well.

d) Layered Surface Structure

The only thermal model investigated which could account for the sustained high heating rates observed for J1, J2, and J3, was one in which a thin (mm) insulating layer covers a highly conductive sub-surface. It is impossible to say whether other models, which have not come to mind, could also explain the observed behavior. We can, however, claim that the two-layer model is simple, plausible, and adequate to explain the data. If the model is essentially a true picture of the surfaces of J1, J2, and J3, the question remains, to what extent is the boundary between the two layers sharp? The same eclipse curves could undoubtedly be generated from a model with an extremely steep gradient in the thermal conductivity with depth. The only requirement is that the conductivity should increase by a factor between 1,000 and 10,000 over a distance of 2-3 millimeters. Although such a gradient can be introduced into a thermal model, in reality it amounts to a fairly sharp boundary between two materials of widely different thermal conductivity.

e) Surface Pressure

Because of the high γ - values inferred for J1, J2, and J3, it is unlikely that the surface pressure, P_s , exceeds 1 mbar on either of these satellites. The results of this study, relating to the question of atmospheres, are therefore the following (1) The upper limit ($P_s < 1$ mbar) set for J3 by Murray, Westphal, and Wildey (1965) is confirmed. (2) The upper

limit ($P_s < 10^{-3}$ mbar) set for J1 by Taylor, et al. (1972) is supported. (3) An upper limit ($P_s < 1$ mbar) for J2 has been determined for the first time.

f) Concluding Remarks

The thermal conductivity of the surface material of J1 is greater than that of either J2 or J3 by a factor of almost 10, from which we have concluded that the surface material on J1 is fundamentally different from J2's and J3's. Since the surface material on J4 is different from any of the inner three satellites (its geometric albedo, phase function, and opacity is lunar-like), there are at least three distinct types of surface material on these four satellites, presumably formed in the same environment. In spite of such differences there are two striking similarities: The emissivity ratio, $\epsilon_{20} / \epsilon_{10}$, is low for all four satellites and, in contrast to the Moon, at least the three inner satellites are covered by thin (mm) layers of particulate material.

Because the similarities are not likely to be of genetic origin, due to the differences discussed above, it seems plausible that they indicate environmental control over some surface conditions. If so, perhaps we are holding a new key to understanding the Jovian environment.

g) Future Work

The findings in this thesis have suggested that the following lines of investigation should be fruitful:

1) The spectral emissivities between 10μ and 30μ should be determined by narrow band photometry. J3 and J4 are most suitable targets for the first attempt because (i) they are the brightest (I.R.) of the four satellites, and (ii) they exhibit very little orbital phase angle variation.

2) The large difference found between the thermal conductivity of J1 and that of J2 or J3 is important, and should be confirmed. 20μ eclipse photometry of these three satellites have been obtained by Morrison (1972) and will be published in 1972. If the 10μ and 20μ eclipse data are to be compared, the reader should be reminded that both sets are normalized to the pre- or post- eclipse flux value. Therefore, a necessary condition of compatibility between the normalized 10$\mu$and 20μ data is that the 20μ flux just prior to eclipse reappearance should be approximately equal to the square root* of the 10μ flux. In other words, if the pre-heating 10μ flux level from J1 is 35%, we should expect the 20μ flux level to be $\approx$ 60 %. Note that this compatibility condition holds for J3 (Figures 15 and 16).

3) Beginning with the 1972 apparition of Jupiter, J4 will also be eclipsed. The next few years therefore offer an ideal opportunity to investigate the surface material of J4.

$$^{*}F_{20} \approx \exp\left[\frac{\gamma}{20\mu}\left(\frac{1}{T_o}-\frac{1}{T}\right)\right] = \exp\left[\frac{\gamma}{10\mu}\left(\frac{1}{T_o}-\frac{1}{T}\right)\right]^{\frac{1}{2}} \approx F_{10}{}^{\frac{1}{2}} \qquad (56)$$

4) We do not believe, however, that the surface materials on the Galilean satellites can be definitely identified by further observations. The breakthrough more likely will come from extensive laboratory work on a few specific compounds. By applying the constraints developed in this and previous work, as well as constraints imposed by chemical equilibria considerations, we should be able to narrow down the range of possible surface materials.

VI. APPENDICES

a) Numerical Technique for Thermal Model

We have shown that the thermal parameters, k and ρc, are virtually independent of temperature for the Galilean satellites. We have therefore been able to use an implicit solution technique described in detail by Burnett (1971). The only significant modification made is that we have applied the solution to a finite surface layer, by holding the temperature constant at the bottom of that layer. This approach is applicable to a thermal model which has a thin upper layer of insulating material (powder or frost) covering a highly conductive (solid rock or ice) subsurface. Such a model is justified in Part IV, section d. Assuming an absence of important, internal heat sources, the equations are:

$$\varepsilon\sigma T^4_{x=o} = (1-A)\,S_\odot \times f(t) + k\frac{\partial T}{\partial x}\bigg|_{x=0} \qquad (57a)$$

$$\rho c\frac{\partial T}{\partial t} = k\frac{\partial^2 T}{\partial x^2} \qquad (57b)$$

$$T(x=\tau, t) = T_o \qquad (57c)$$

$$T(x,o) = T_o \qquad (57d)$$

f(t) is the normalized insolation function, and τ is the thickness of the insulating layer.

Numerical Solution:

Let $t = (j-1)\,\Delta t$ (58a)

$x = (i-2)\,\Delta x$ (58b)

$T(x=0, t=0) = T_{2,1}$ (58c)

Note that $T_{1,j}$ is a fictitious temperature in the void, one Δx-step above the surface, and that $T_{2,j}$ is the surface temperature as a function of time.

Define:

$$k_1 = \Delta t k/\rho c \Delta x^2 \qquad (59a)$$

$$k_2 = 2/k_1 + 2 \qquad (59b)$$

$$k_3 = 2/k_1 - 2 \qquad (59c)$$

$$k_4 = 2k_1/k_2 \qquad (59d)$$

$$k_5 = 2k_1\Delta x(1-A)/k \qquad (59e)$$

$$k_6 = 2\Delta x \epsilon \sigma/k \qquad (59f)$$

$$k_7 = k_5/k_1 \qquad (59g)$$

$$g_1 = k_1 \times k_6 \qquad (59h)$$

$$g_2 = k_1(k_2 - 2/k_2) \qquad (59i)$$

Then, for each time step (j), the solution for temperature with depth is given by the following matrix equation:

$$\begin{bmatrix} 2 & -k_2 & 0 & 0 & 0 & 0 & 0 & 0 \\ -1 & k_2 & -1 & 0 & 0 & 0 & 0 & 0 \\ 0 & -1 & k_2 & -1 & 0 & 0 & 0 & 0 \\ & & & \cdot & & & & \\ & & & & \cdot & & & \\ & & & & & \cdot & & \\ 0 & 0 & 0 & 0 & -1 & k_2 & -1 & 0 \\ 0 & 0 & 0 & 0 & 0 & 1 & -4 & 3 \\ 0 & 0 & 0 & 0 & 0 & 0 & 0 & 1 \end{bmatrix} \times \begin{bmatrix} T_{1,j} \\ T_{2,j} \\ T_{3,j} \\ \cdot \\ \cdot \\ \cdot \\ T_{m-2,j} \\ T_{m-1,j} \\ T_{m,j} \end{bmatrix} = \begin{bmatrix} R_{1,j} \\ R_{2,j} \\ R_{3,j} \\ \cdot \\ \cdot \\ R_{m-2,j} \\ R_{m-1,j} \\ R_{m,j} \end{bmatrix} \qquad (60)$$

where the R-vector, given below, must be computed for each time step. Note that the square matrix contains no time dependent quantities, and can be inverted before any computations are made. This is the great advantage in being able to use constant thermal parameters. Having inverted the square matrix, the T-vector (i.e. the temperature with depth) is computed as follows:

(i) Compute the R-vector

$$R_{i,j} = T_{i-1,j-1} + k_3 T_{i,j-1} + T_{i+1,j-1} \qquad i \neq 1,m \qquad (61a)$$

$$R_{m,j} = T_o \qquad (61b)$$

(ii) Let $g_3 = k_4(k_1 R_{4,i} + R_{3,i} - T_{4,i-1}) + k_1 R_{2,i} + k_5 S_\odot f(t)$ (62)

and $\tilde{T}(n=1) = T_{2,i-1}$ (63)

then iterate over "n" to obtain a first estimate of the new surface temperature, $T_{2,i}$, according to

$$\tilde{T}(n) = [3g_1\tilde{T}^4(n-1) + g_3] \Big/ [4g_1\tilde{T}^3(n-1) + g_2] \quad . \tag{64}$$

When $\tilde{T}(n) \approx \tilde{T}(n-1)$, stop the iteration, and set $T_{2,i} = \tilde{T}(n)$. This will give a first estimate of the new surface temperature, subject to slight modification in the final solution.

(iii) Evaluate $R_{1,i} = k_7 S_\odot f(t) - k_6 T^4_{2,i} - R_{2,i}$ (65)

(iv) Compute the new T_i-vector.

The time steps were taken to be 1 minute each in order to provide good resolution over the 20 minute heating history, and the depth steps were taken to be 1/12 the thermal skin depth, L, for the homogeneous model, and 1/12 the thickness of the insulating layer in the two-layer model. The thermal skin depth is given by

$$L \approx (k\Delta t/\rho c)^{\frac{1}{2}} \text{ where } \Delta t \approx 20 \text{ min.} \tag{66}$$

This "grid" was found empirically to be adequate in the sense that decreasing the grid spacings did not alter the solution.

b) Tests of Model Assumptions

Of the four assumptions made in the thermal model, two have been tested for J1 after the determination of the correct model parameters. The results are discussed below

(i) Treating the Satellite as a Flat Disk

The "flat disk" model, in which the actual temperature distribution is

replaced by an "effective temperature" defined by

$$B(\lambda, T_{eff}) = 2\int_0^{\pi/2} B[\lambda, T(\theta)] \cos\theta \sin\theta \, d\theta \quad , \tag{67}$$

has been compared to a model which accounted for spherical geometry and actual temperature distribution. The second model was also crude in the sense that 5 equally sized (in terms of projected area), concentric integration cells were used to represent the hemisphere. Nevertheless, it is much more realistic than the "flat disk" model. The result of the comparison, shown in Figure 20, was that there were no essential differences in the predictions of the two models. We may therefore assume that the "flat disk" model is adequate for modeling eclipses.

(ii) Simultaneous Eclipse over Entire Satellite Disk

If the satellite moves its own diameter relative to Jupiter's shadow in a time short compared to the time required to heat up the surface at any particular place, we may assume that the eclipse occurs simultaneously over the entire satellite disk. The ratios of these periods for J1, J2, and J3 are: $3.5/20 \approx 0.18$, $3.8/25 \approx 0.22$, $8.4/28 \approx 0.28$. As a test case, the disk of J1 was divided into 7 vertical strips. Each strip was assigned a flux proportional to its area and given a time dependence similar to the observed integrated flux, but offset in time in the obvious manner. The flux sum from the strips was found and plotted as a function of time together with the flux from a uniform disk. The results are shown in Figure 20, and show that eclipses may be assumed to occur simultaneously over the entire satellite disk.

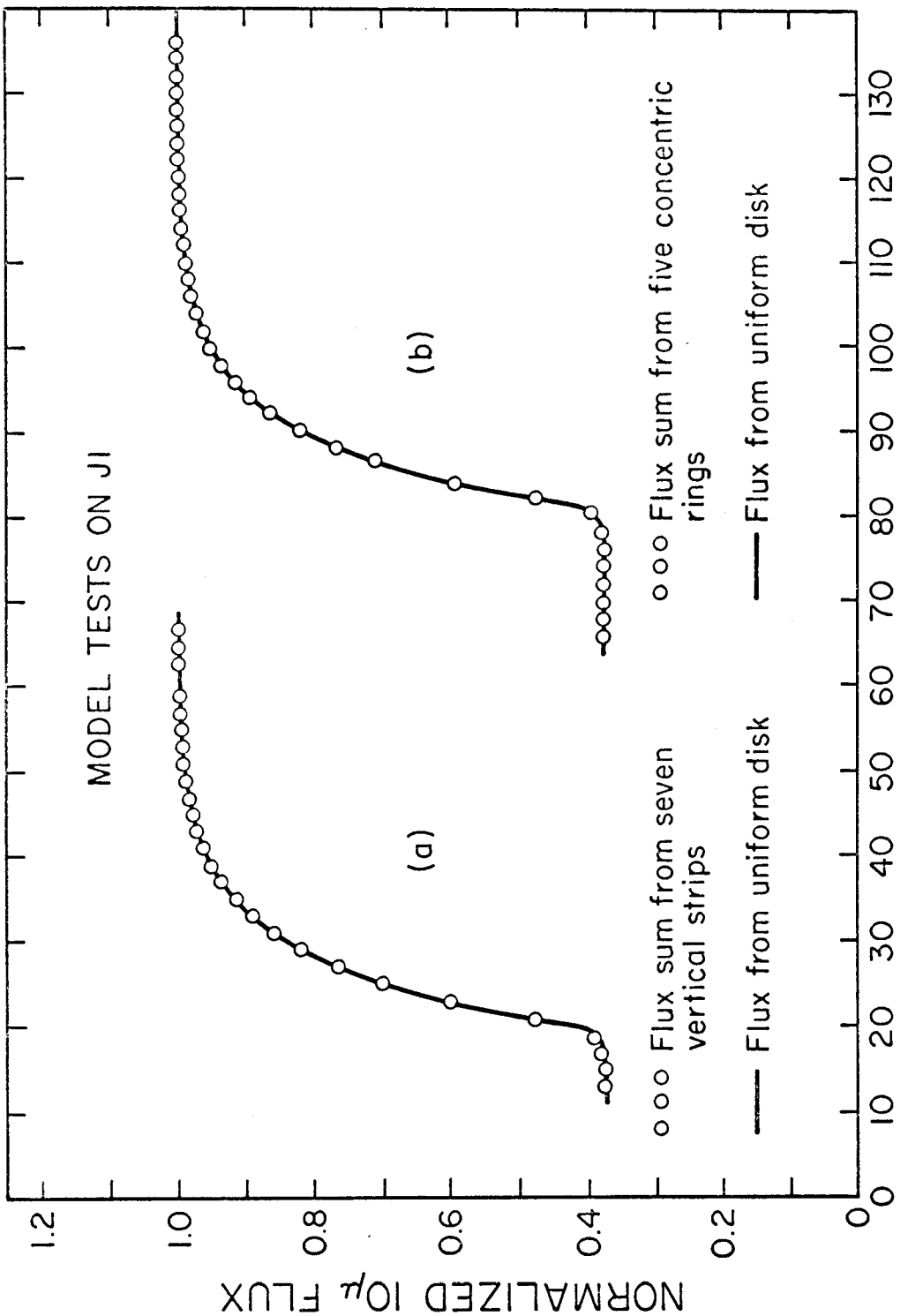

Fig. 20. - (a) Test for simultaneous eclipse assumption. (b) Test for disk v/s spherical geometry assumption.

c) Mie-Scattering and Emissivity

Conel (1969) has developed a model for the infrared emissivity of particulate materials, and applied it to a study of silicate powders in the wavelength region from 7μ to 15μ. His model involves two free parameters: the single scattering albedo, ω_o, and the mean assymmetry factor, $\langle\cos(\theta)\rangle$. In the model, the spectral emissivity is given by

$$\epsilon(\lambda) = 1/(1+\upsilon) \tag{68}$$

where

$$\upsilon = \left(\frac{1 - \omega_o\langle\cos\theta\rangle}{1 - \omega_o}\right)^{\frac{1}{2}} . \tag{69}$$

ω_o and $\langle\cos\theta\rangle$, both of which are wavelength dependent, may be determined for a given material, from Mie-scattering theory, if its real and imaginary indices of refraction and its absorbsion coefficient are known as functions of wavelength. The calculation is extremely complicated, and has not been attempted here. However, Irvine and Pollack (1968) have carried out the calculation for water and ice spheres with radii 0.3, 1.0, 3.0, and 10.0μ, and have tabulated values of ω_o and $\langle\cos\theta\rangle$ for $1\mu < \lambda < 200\mu$. Assuming Irvine and Pollack's (1968) table and Conel's (1969) formula, $\epsilon(\lambda)$ has been calculated for ice spheres of the given radii, and plotted in Figure 21. Note the pronounced dip in the emissivity at 20μ for particle radius equal to 10μ.

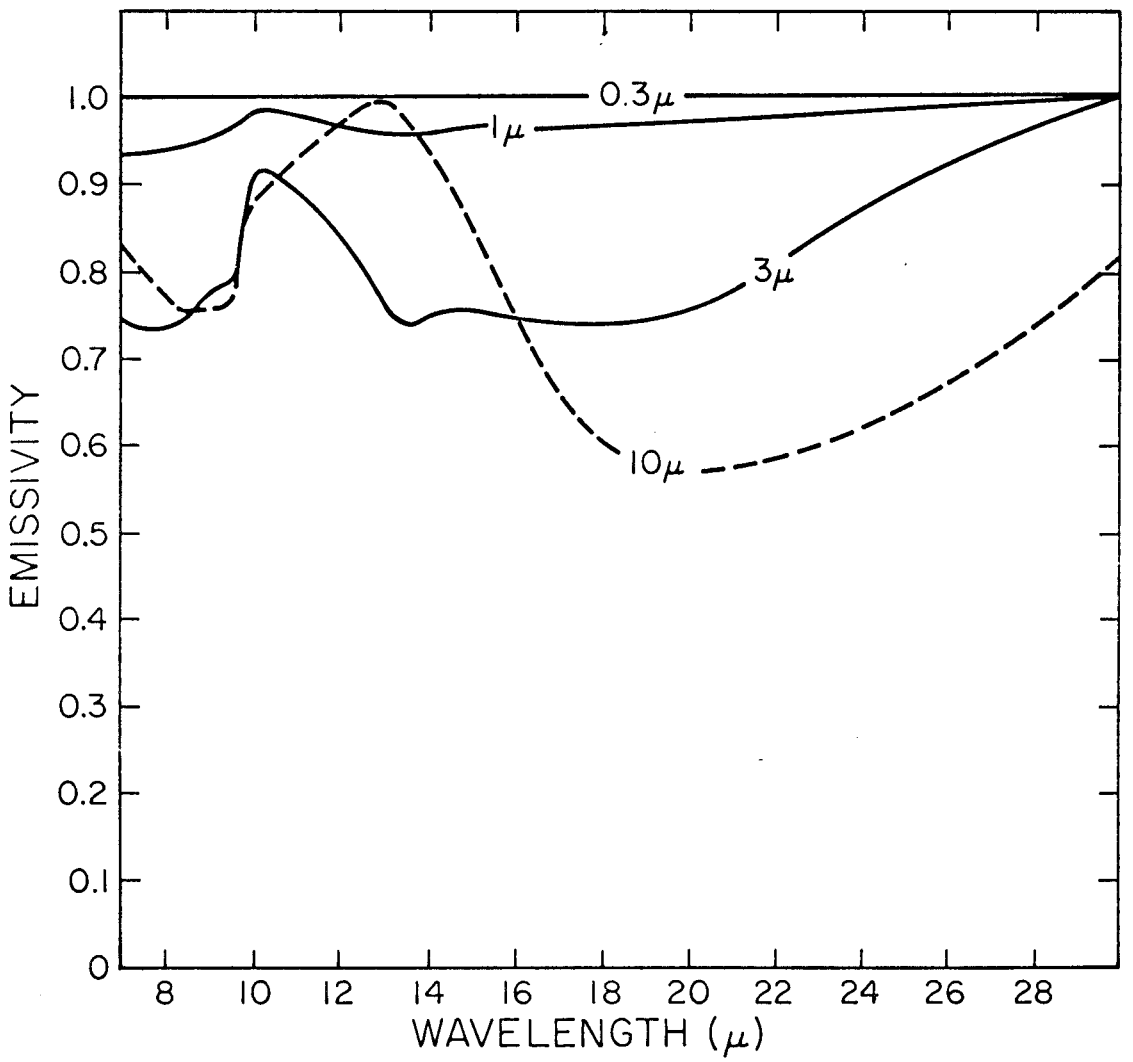

Fig. 21 - Calculated emissivity of ice spheres, with radii r = 0.3, 1, 3, 10.0μ, as a function of wavelength.

d) Bandpasses

The 10 and 20μ bandpasses are shown in Figure 22. In calculating the bandpasses, the filter, atmosphere, and window transmissions were accounted for.

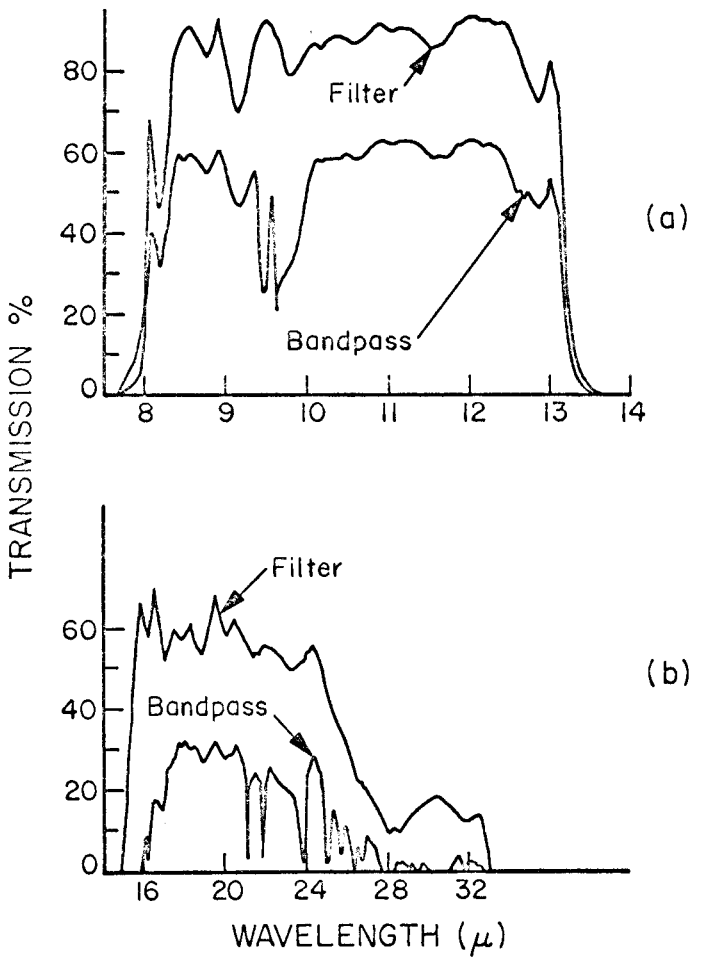

Fig. 22 - (a) 10μ bandpass, (b) 20μ bandpass.

REFERENCES

Allen, D.A. 1971, "Infrared Studies of the Lunar Terrain" The Moon 2 320 - 337

Arvesen, J.C., Griffin, R.N. and Pearson, B.D. Jr. 1969, "Determination of Extraterrestrial Solar Spectral Irradiance from a Research Aircraft", App. Optics 8 2215-2232

Bastin, J.A. and Gough, D.O. 1969, "Intermediate Scale Lunar Roughness", Icarus 11 289-319

Bigg, E.K. 1964, "Influence of the Satellite Io on Jupiter's Decametric Emission", Nature 203 1008-1010

Binder, A.B. and Cruikshank, D.P. 1964, "Evidence for an Atmosphere on Io", Icarus 3 299-305

Binder, A.B. and Cruikshank, D.P. 1966, "On the Spectra of the Galilean Satellites of Jupiter", Ap. J. 144 L 1240-1241

Binder, A.B. and Cruikshank, D.P. 1966, "Photometric Search for an Atmosphere on Europa and Ganymede", Icarus 5 7-9

Birkebak, R.C. and Cremers, C.J. 1970, "Thermal Radiation Properties and Thermal Conductivity of Lunar Material", Science 167 724-726 Sample 10084-68, 2

Burnett, G.B. III, 1971, "The Surface Temperatures of Solar System Objects by Thermal Emission: A Homogeneous Model Solution", M.S. Thesis, School of Physics and Astronomy, University of Minnesota

Conel, J.E. 1969, "Infrared Emissivities of Silicates: Experimental Results and a Cloudy Atmosphere Model of Spectral Emission from Condensed Particulate Mediums", J.G.R. 74 1614-1634

Dean, J.W. and Timmerhaus, K.D. 1962, "Thermal Conductivity of Solid H_2O and D_2O at Low Temperature", Advances in Cryogenic Engineering 8 263

de Sitter, W. 1931, "Jupiter's Galilean Satellites",MNRAS 91 706

Dollfus, A. 1970, "Diametres des Planetes et Satellites", in Surfaces and and Interiors of Planets and Satellites Ch.2, Dollfus, Ed. Academic Press

Dyal, P. and Parkin, C.W. 1971, "Electrical Conductivity and the Temperature of the Lunar Interior from Magnetic Transient - Response Measurements", J.G.R. 76 5947-5969

Fallon, F.W. and Murphy, R.E. 1970, "Absence of Post-eclipse Brightening of Io and Europa in 1970", Icarus 15 492-497.

Farmer, C.B. and Key, P.J. 1965, " A Study of the Solar Spectrum from 7μ to 400μ " App. Optics 4 1051-1068

Fountain, J.A. and West, E.A. 1970, "Thermal Conductivity of Particulate Basalt as a Function of Density in Simulated Lunar and Martian Environments", JGR 75 4063-4069

Franz, O.G. and Millis, R.L. 1970, " A Search for an Anomalous Brightening of Io after Eclipse", Icarus 14 13

Gehrels, T. 1956, "Photometric Studies of Asteroids, V. The Light-Curve and Phase Function of 20 Massalia." Ap. J. 123 331-338

Gehrels, T., Coffeen, T., and Owings, D. 1964, "Wavelength Dependence of Polarization III. The Lunar Surface", Astron. J. 69 826-852

Gillett, F.C., Merrill, K.M. and Stein, W.A. 1970, "Albedo and Thermal Emission of Jovian Satellites I - IV ", Astrophysical Letters 6 247-249

Goldreich, P. and Lynden-Bell, D. 1969, "Io, a Jovian Unipolar Inductor", Ap. J. 156 59-78

Greene, T.F., Shorthill, R.W. and Despain, L.G. 1971, " Jovian Satellites Eclipse Study I ", Boing Scientific Research Laboratory, Report: D1 - 80-14193-1

Griggs, M. 1968, "Emissivities of Natural Surfaces in the 8- to 14 - Micron Spectral Region", JGR 73 7545-7551

Gromova, L.V., Moroz, V.I. and Cruikshank, D.P. 1970, "The Spectrum of Ganymede in the Region 1-1.7 Microns", Astronomicheskii Tsirkular (Astronomical Circular) No. 569 USSR.

Hapke, B. and Van Horn, H. 1963, "Photometric Studies of Complex Surfaces, with Applications to the Moon", J.G.R. 68 4545-4570. See Appendix p.4569

Hapke, B. 1963, "A Theoretical Photometric Function for the Lunar Surface", J.G.R. 68 4571-4586

Hapke, B. 1966, "An Improved Theoretical Lunar Photometric Function", Astron. J. 71 333-339

Harris, D.L. 1961, "Photometry and Colorimetry of the Planets and Satellites", in Planets and Satellites G.P. Kuiper and B.M. Middlehurst, eds. ch.8, University of Chicago Press, Chicago

Horai, K., Simmons, G., Kanamori, H. and Wones, D. 1970, "Thermal Diffusivity and Conductivity of Lunar Material", Science 167 730-731

Hunt, G.R. and Logan, L.M. 1972, "Variation of Single Particle Mid-Infrared Emission Spectrum with Particle Size", Applied Optics 11 142-147

Irvine, W.M. and Pollack, J.B. 1968, "Infrared Optical Properties of Water and Ice Spheres." Icarus 8 324-360

Johnson, T.V. and McCord, T.B. 1970, "Galilean Satellites The Spectral Reflectivity 0.30-1.10 Micron", Icarus 13 32-42

Johnson, T.V. and McCord, T.B. 1971, "Spectral Geometric Albedo of the Galilean Satellites, 0.3 to 2.5 Microns", Ap. J. 169 589-594

Johnson, T.V. 1971, "Galilean Satellites:Narrowband Photometry 0.30 to 1.10 Microns", Icarus 14 1-18

Kalinyak, A.A. 1966, "Data on the Spectra of the Galilean Satellites of Jupiter", Soviet Astron. A.J. 9 824-825

Keegan, H.J. and Weidner, V.R. 1966, "Infrared Spectral Reflectance of Frost", Optical Soc. of America 56 523-524

Kuiper, GP. 1952, in The Atmospheres of the Earth and Planets (Rev. ed.) Kuiper, G.P., ed., University of Chicago Press, p.368

Labs, D. and Neckel, H. 1971, "The Solar Constant", Solar Physics 19 3-15

Lewis, J.S. 1971, "Satellites of the Outer Planets: Their Physical and Chemical Nature", Icarus 15 174-185

Linsky, J.L. 1966, "Models of the Lunar Surface Including Temperature-Dependent Thermal Properties", Icarus 5 606-634

Low, F.J. 1965, "Planetary Radiation at Infrared and Millimeter Wavelengths", Lowell Obs. Bull 6 184-187

Marsden, B. 1971, Private communication on mass determinations of the Galilean satellite. M2 is well determined. M3 is probably O.K. M1 and M4 are very doubtful. Smithsonian Inst. Astrophysical Obs., Cambridge, Mass.

Matson, D.L. 1972, "(1) Astronomical Photometry at Wavelengths of 8.5, 10.5 and 11.6 μm (2) Infrared Emission from Asteroids at Wavelengths of 8.5, 10.5 and 11.6 μm.", Ph.D. Thesis California Institute of Technology

McNamara, D.H. 1964, "Narrowband Photometry of Stars, Planets and Satellites", North American Aviation, Inc., Space and Information Systems Division, SID 64-78, Accession No. No. 52156-64

Merrill, R.B. 1968, "Measurements of the Thermal Conductivity of Glass Beads in a Vacuum at Temperatures from 100° to 500° K", Thermal Conductivity. Proceedings of the 7th Conference. Flynn, D.R. and Peavy, B.A. Jr. eds. Nat. Bur. of Stand. Special Publication 302

Minnaert, M. 1961, "Photometry of the Moon", in Planets and Satellites, Kuiper, G. and Middlehurst, M. eds. The University of Chicago Press, pp213-248

Moroz, V.I. 1966, "Infrared Spectrophotometry of the Moon and the Galilean Satellites of Jupiter", Soviet Astron. - A.J. 9 999-1006

Morrison, D., Cruikshank, D.P., Murphy, R.E., Martin, T.Z. Beery, J.G. and Shipley, J.P. 1971, "Thermal Inertia of Ganymede from 20- Micron Eclipse Radiometry", Ap. J. 167 L107-111

Morrison, D., Cruikshank, D.P. and Murphy, R.E. 1972, "Temperatures of Titan and the Galilean Satellites at 20 Microns", Preprint. U. of Hawaii

Morrison, D. 1972, Private communication on eclipse observations of J1 and J2. During the 1971 apparition of Jupiter, Morrison, et al. obtained 20μ and this author obtained 10μ eclipse data on J1 and J2. Institute for Astron. U. of Hawaii, Honolulu, Hawaii

Murray, B.C., Wildey, R.L. and Westphal, J.A. 1964, "Observations of Jupiter and the Galilean Satellites at 10 Microns", Ap. J. 139 986-993

Murray, B.C., Westphal, J.A. and Wildey, R.L. 1965, "The Eclipse Cooling of Ganymede", Ap. J. 141 L1591-1592

Neugebauer, G., Munch, G., Kieffer, H., Chase, S.C.Jr., and Miner, E. 1971, "Mariner 1969 Infrared Radiometer Results: Temperatures and Thermal Properties of the Martian Surface", Astron. J. 76 719-728

Neugebauer, G., Becklin, E.E. and Hansen, O.L. 1972, "Absolute Flux Calibration of Alpha Scorpii at 10 and 20 Microns", To be published.

Oetking, P. 1966, "Photometric Studies of Diffusely Reflecting Surfaces with Application to the Brightness of the Moon", J.G.R. 71 2505

Oke, J.B. and Schild, R.E. 1970, "The Absolute Spectral Energy Distribution of Alpha Lyrae", Ap. J. 161 1015-1023

O'Leary, B. and Veverka, J. 1970, "On the Anomalous Brightening of Io after Eclipse", Preprint. Laboratory for Planetary Studies, Center for Radiophysics and Space Research, Cornell University, Ithaca, N.Y. 14850

Owen, T. 1965, "Saturn's Rings and the Satellites of Jupiter", Science 149 974

Price, M.J. and Hall, J.S. 1971, "The Physical Properties of the Jovian Atmosphere Inferred from Eclipses of the Galilean Satellites. I. Preliminary Results", Icarus 14 3-12

Saari, J.M. and Shorthill, R.W. 1967, "Review of Lunar Infrared Observations", in Physics of the Moon Singer, S.F. ed. 13 57-99. Science and Technology Series, American Astronautical Society.

Schild, R., Peterson, D.M. and Oke, J.B. 1971, "Effective Temperatures of B- and A- Type Stars", Ap. J. 166 95-108

Stebbins, J. 1927, "The Light-Variations of the Satellites of Jupiter and their Application to Measures of the Solar Constant", Lick Obs. Bull. 13 1-11

Stebbins, J. and Jacobsen, T.S. 1928, "Further Photometric Measures of Jupiter's Satellites and Uranus, with tests of the Solar Constant", Lick Obs. Bull. 13 180-187

Taylor, G.E., O'Leary, B., Van Flandern, T.C., Smith, B.A., Smith, S.A., Fallon, F.W., Devinney, E.J., and Oliver, J. 1972," "Occultation of Beta Scorpii C by Io on May 14, 1971", Nature 234 405-406

Van Diggelen, J. 1965, "The Radiance of Lunar Objects Near Opposition" Planet. Space Sci. 13 271-279

Veverka, J. 1970, "Photometric and Polarimetric Studies of Minor Planets and Satellites". Ph.D. Thesis, Harvard

Veverka, J. 1971, "Polarization Measurements of the Galilean Satellites of Jupiter", Icarus 14 355-359

Watson, K. 1964, "The Thermal Conductivity Measurements of Selected Silicate Powders in Vacuum from 150° - 350° K " Ph.D. Thesis, California Institute of Technology, Pasadena, California

Wechsler, A.E. and Glaser, P.E. 1965, "Pressure Effects on Postulated Lunar Materials" Icarus 4 335-352

Wechsler, A.E. and Simon, I. 1966, "Thermal Conductivity and Dielectric Constant of Silicate Materials", Final Report under NASA Contract NAS 8-20076

Wessellink, A.J. 1948, "Heat Conductivity and Nature of the Lunar Surface Material", Bull. Astr. Inst. Netherlands 10 351

Winter, D.F. and Saari, J.M. 1969, "A Particulate Thermophysical Model of the Lunar Soil", Ap. J. 156 1135-1151